Design of flexible MOF-508 for optimal gate pressures for acetylene safe storage

Mickaele Bonneau[1], Christophe Lavenn[2], Kunihisa Sugimoto[1,3], Alexandre Legrand[1], Tomofumi Ogawa[2], Francois-Xavier Coudert[4], Regis Reau,[5] Ken-ichi Otake[1] & Susumu Kitagawa[1]

1 Institute for Integrated Cell-Material Sciences (WPI-iCeMS), Kyoto University, Sakyo-ku, Kyoto 606- 8501, Japan

2 Air Liquide Laboratories, Innovation campus Tokyo, 2-2 Hikarinooka, Yokosuka, Kanagawa, 239-0847 Japan

3 Japan Synchrotron Radiation Research Institute/ SPring-8, Kouto, Sayo, Hyogo 679-5198, Japan

4 Chimie ParisTech, PSL University, CNRS, Institut de Recherche de Chimie Paris, 75005 Paris, France

5 Air Liquide R&D, Innovation Campus Paris 1, Chemin de la Porte des Loges 78350 Les Loges-en-Josas, France.

Supplementary Methods.

General instrumental analysis

^{1}H NMR spectra

All IML-MOFs were dissolved in 0.75 mL of DMSO-d^6 and 10μL of deuterated TFA. ^{1}H NMR spectra were recorded at 25 °C at 400MHz, where chemical shifts (δ in ppm) were determined with respect to tetramethylsilane (TMS) as an internal reference.

Thermal stability of all MOFs were measured under nitrogen flux with a heating rate of 5 °C min^{-1} from 30 to 500 °C on a Perkin Elmer STA 6000 Thermo Gravimetric Analyzer (TGA).

Powder X-ray diffraction (PXRD) measurements were performed on a Rigaku SmartLab X-ray diffractometer using Cu−Kα radiation (λ = 1.54178 Å) in the 2θ range of 3−40° with a scanning rate of 5 ° min^{-1}.

UV analysis of all materials were measured on a JASCO V670 spectrophotometer from 700 to 200 nm. Samples were previously heated at 423 K under vacuum for 12 h before measurements.

SEM analysis Scanning electron microscopy (SEM) images were collected with HITACHI SU5000 microscope using 3.0 kV acceleration voltage and 5 mm working distance. Samples were directly deposited on a carbon conductive carbon tape.

Single crystal X-ray diffraction

Measurements of single crystal X-ray diffraction data for as-synthesized and activated **$(NO_2)_{100}$-MOF-508** were collected on the beamline BL02B1 at the Japan Synchrotron Radiation Research Institute with 0.41270 Å radiation at 100 K and 195 K respectively. Crystals were extracted from a mixture DMF/EtOH into oil and mounted onto the goniometer for data collection. The structures were solved using *SHELXT*. Structure solution and refinement was performed within *SHELXL* on *Olex2*. Crystal information and details relating to the structural refinements are presented in Supplementary **Table 1 & 2**. Crystallographic data for as-synthesized and activated **$(NO_2)_{100}$-MOF-508** structures have been deposited in the Cambridge Structural Database with CCDC numbers 2036574 -2036575.respectively.

Single gas adsorption isotherms MOF samples were prior activated through thermal activation at 423 K for 12 h before measurement. The adsorption isotherms were measured with BELSORP-CRYO (C_2H_2 and CO_2) and BELSORP-MAX (C_2H_2, CO_2, CH_4 and O_2) volumetric adsorption equipment from Bel Japan. Targeted relative pressures in the range of 0.01-100 kPa were defined

and limits of excess and allowance amount were set to 5 and 10 $cm^3\ g^{-1}$, respectively. Equilibrium conditions for each point were: 0.03% pressure change within 300 s. The dead volume was determined using helium gas.

In-situ PXRD coupled with gas sorption measurements were performed on BELSORP-18PLUS (MicrotracBEL, Japan, Corp.) automated volumetric sorption analyzers, equipped with cryostat temperature controllers. The in-situ PXRD/adsorption measurements were carried out using a Rigaku SmartLab with Cu−Kα radiation connected to BELSORP-18PLUS volumetric adsorption equipment. Those apparatuses were synchronized with each other and each PXRD pattern was obtained at each point of the sorption isotherms. The samples were prior activated through external thermal activation at 423 K for 12 h and further 2 h internal activation at 423 K before measurement.

Materials

All chemicals were used as received without any further purification., 1,4-benzenedicarboxylic acid, 2-amino-1,4-benzenedicarboxylic acid, 2-nitro-1,4-benzenedicarboxylic acid, 4,4´-bipyridine were purchased from TCI. Zinc nitrate hexahydrate, Ethanol (EtOH), dimethylformamide (DMF) and other materials were purchased from Nacalai Tesque.

MOF synthesis MOF-508 and **$(X)_n$-MOF-508**series (***n*** = 0 to 100% and **X** = **NH_2**, **NO_2**) were prepared following a method previously published and can be produced in 100 g scale.[15] 1,4-benzenedicarboxylic acid is dissolved with the functionalized 1,4-benzenedicarboxylic acid (total 2 eq) in DMF (concentration [**bdc linker**] = 0.15 M) at 100 °C for 15 min. An ambient solution of $Zn(NO_3).6H_2O$ (2 eq) in DMF (concentration [**metal**] = 0.4 M) was added to the stirring mixture at 100 °C for 10 min. 4,4´-bipyridine (1 eq) is dissolved at room temperature in EtOH

(concentration [**pillar**] = 0.1 M) and added to the reaction mixture. The mixture was kept at 100 °C for 24 h. After cooling down to room temperature, the resulting precipitated is collected *via* centrifugation and washed three time with DMF (3 x 40 mL) and three times with EtOH (3 x 40 mL). The white/yellow powder is dried under vacuum at 50 °C for 12 h.

Acetylene high pressure storage test set-up measurements The experimental set-up used for acetylene storage measurements is shown in Supplementary **Figure 40**. The gas manifold consisted of two lines fitted with mass flow controller. One line is used to feed an inert gas, in our case helium gas is used as reference gas before each experiment and as gas purge after each acetylene measurement. The other line, contains pure acetylene gas. In a typical experiment, 10 g of adsorbent powder was activated under vacuum at 423 K in a separate oven for 12 h. The vessel is filled with helium and plugged in the set-up. Before starting each experiment, the column is evacuated and heated at 423 K for 2 h before the acetylene filling at a flow rate of 50 $cm^3.min^{-1}$. After filling, the desorption is made by vacuum pump until complete release of the gas.

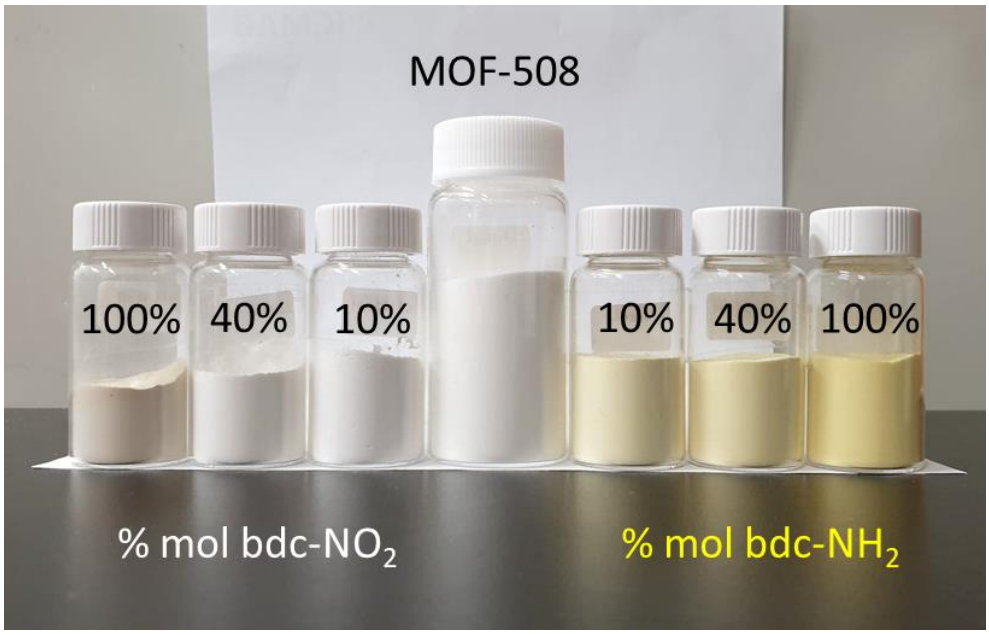

Supplementary **Figure 1**. **$(X)_n$-MOF-508** selection used for this study.

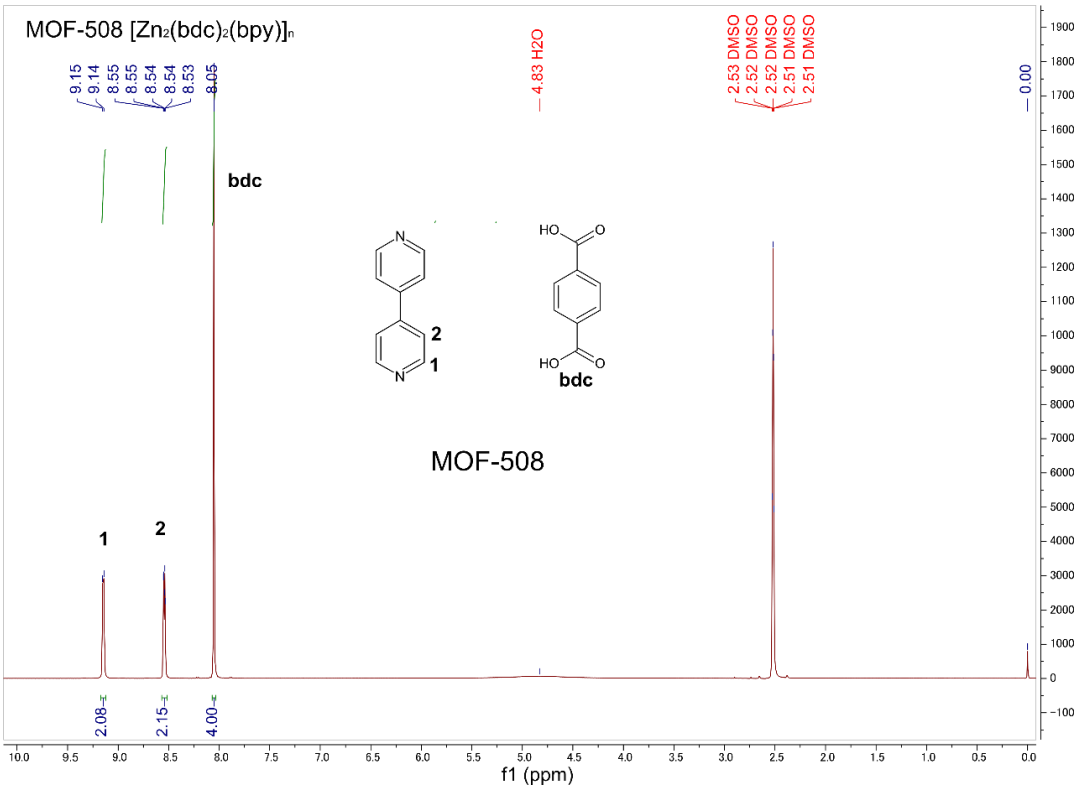

Supplementary **Figure 2 |** ^{1}H-NMR spectra of digested **MOF-508** in DMSO-d^{6}.

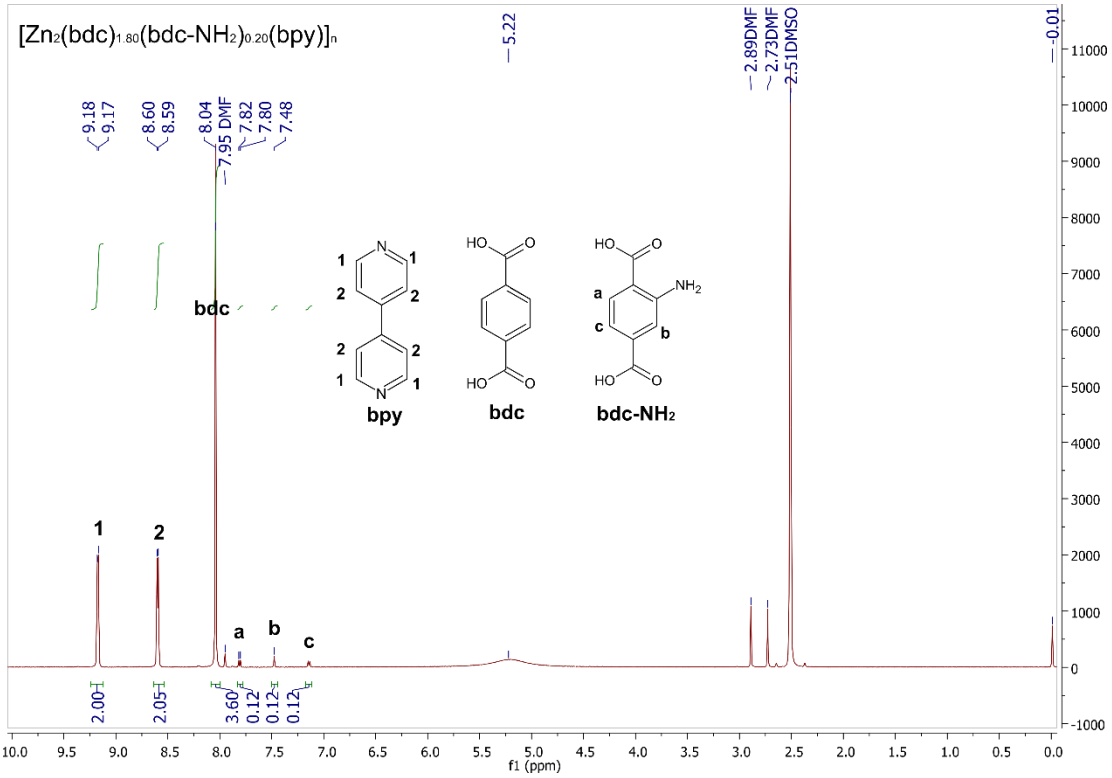

Supplementary **Figure 3 |** ^{1}H-NMR spectra of digested **$(NH_2)_{10}$-MOF-508** in DMSO-d^{6}

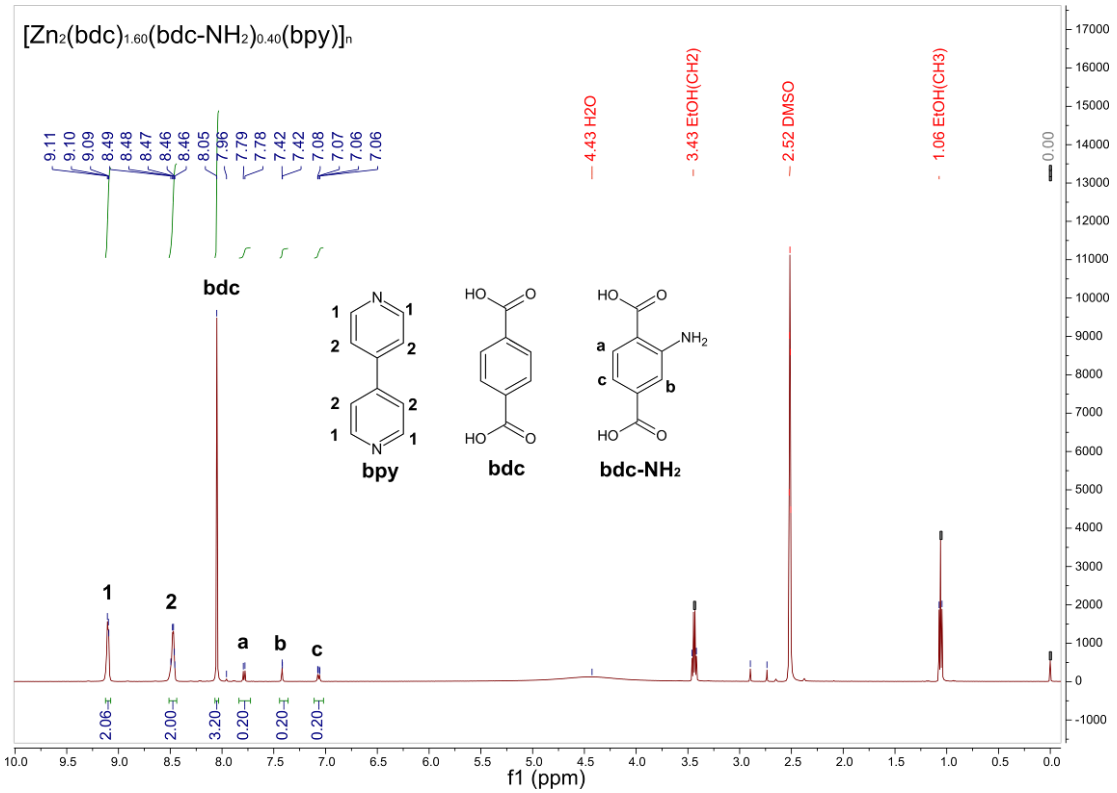

Supplementary **Figure 4 |** ^{1}H-NMR spectra of digested **$(NH_2)_{20}$-MOF-508** in DMSO-d^{6}

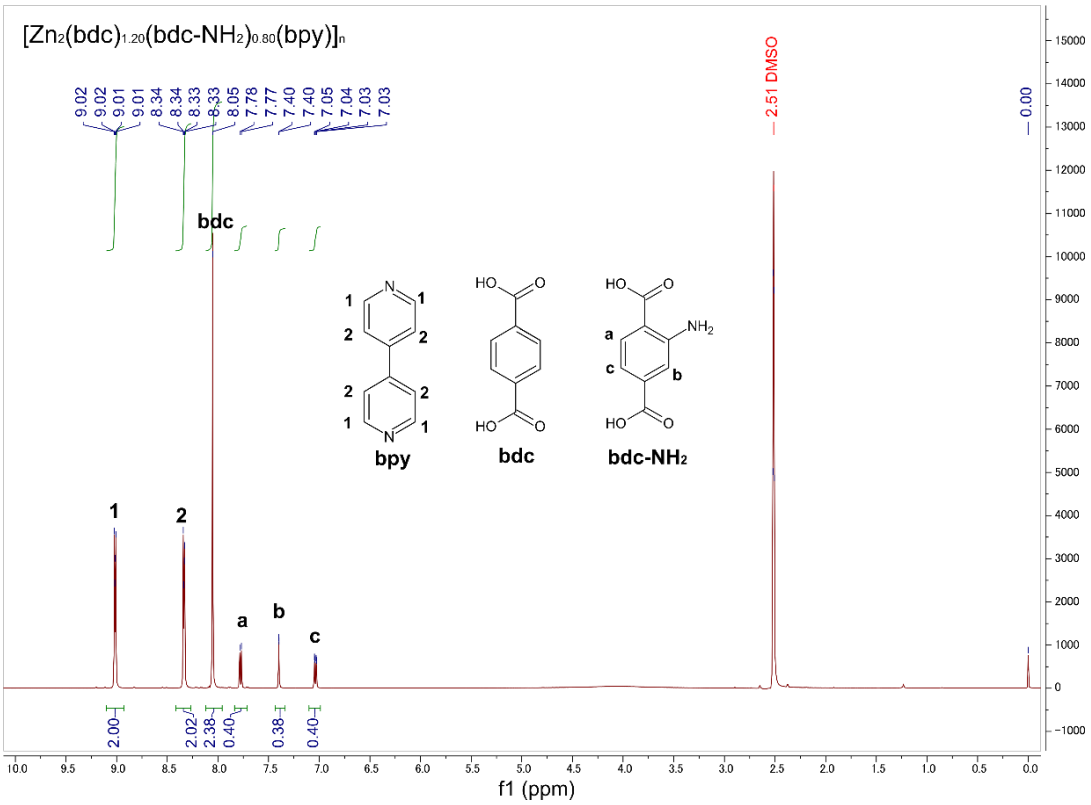

Supplementary **Figure 5 |** ^{1}H-NMR spectra of digested **$(NH_2)_{40}$-MOF-508** in DMSO-d^{6}

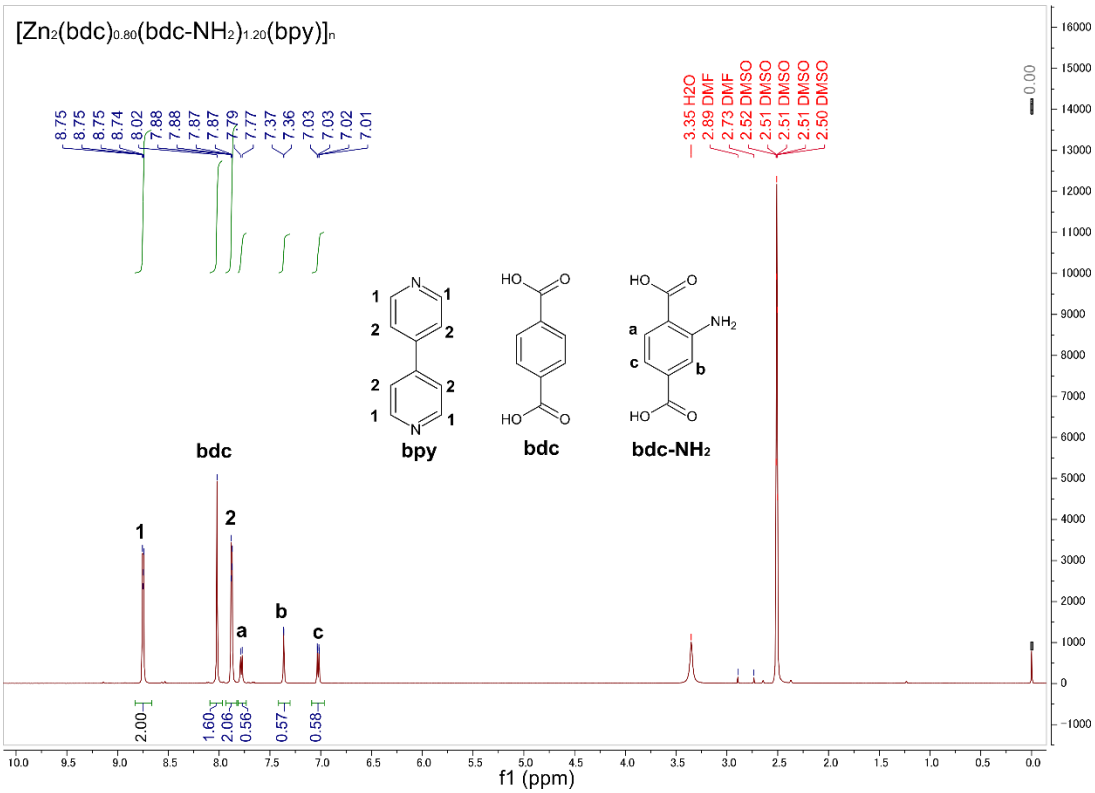

Supplementary **Figure 6 |** ^{1}H-NMR spectra of digested **$(NH_2)_{60}$-MOF-508** in DMSO-d^{6}

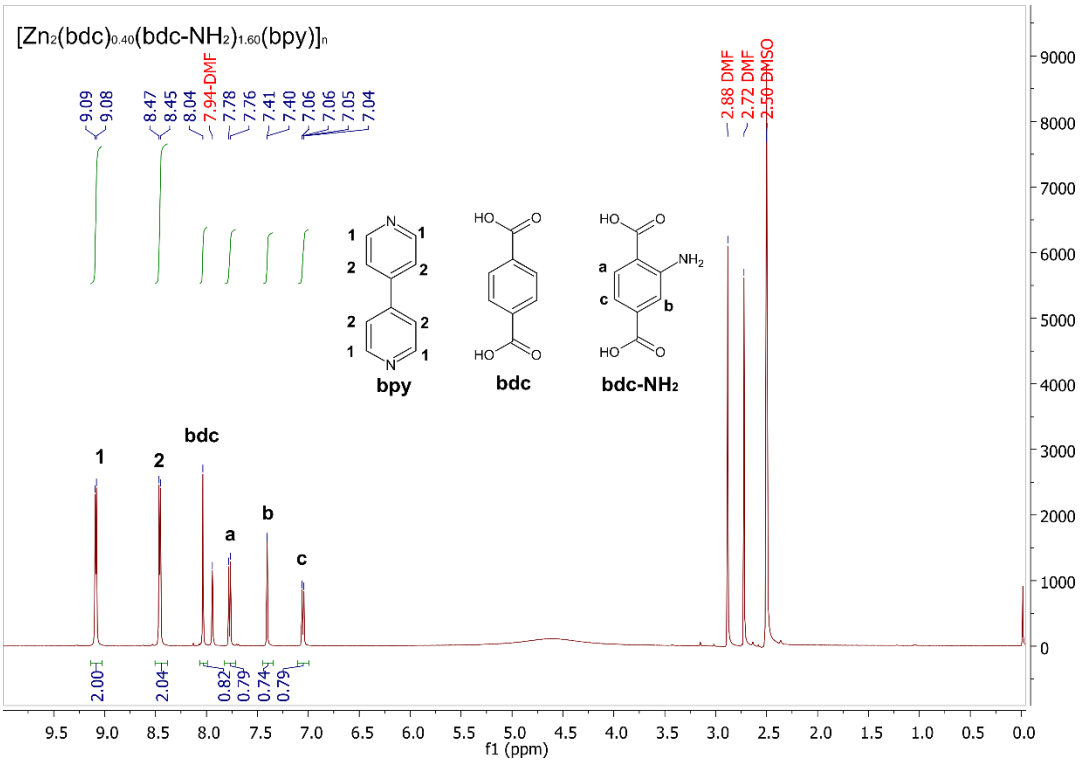

Supplementary **Figure 7 |** ^{1}H-NMR spectra of digested **$(NH_2)_{80}$-MOF-508** in DMSO-d^{6}

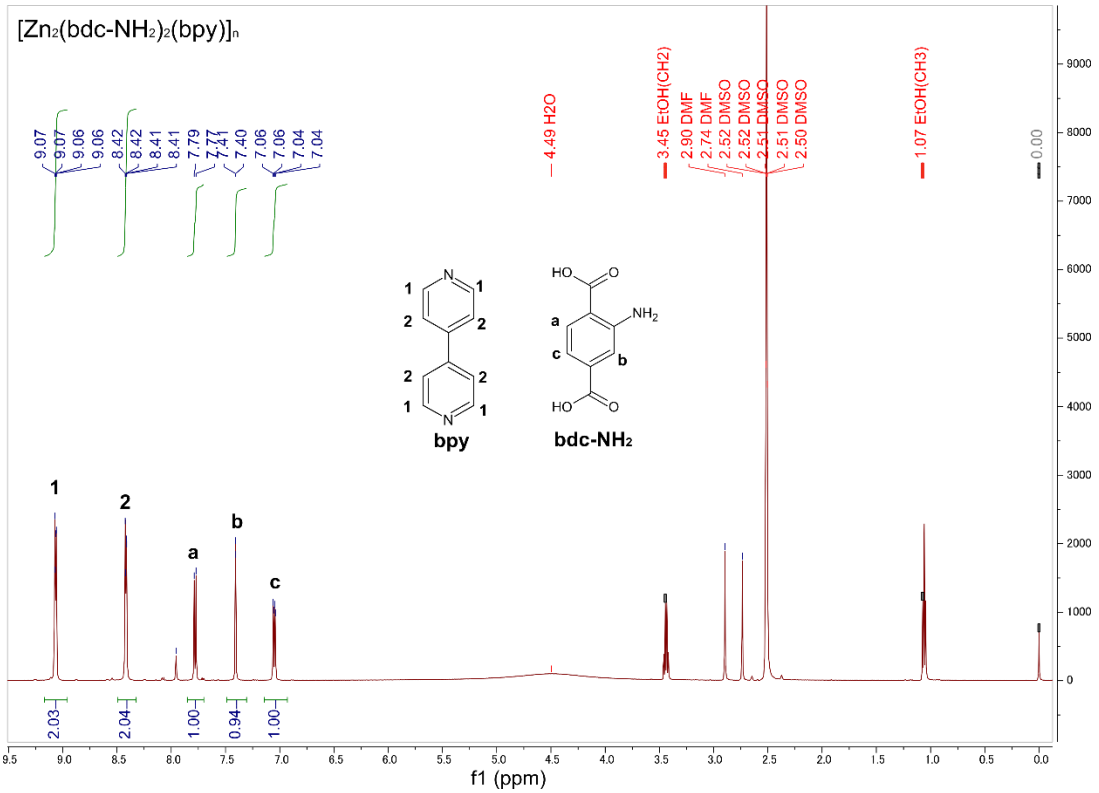

Supplementary **Figure 8** | ^{1}H-NMR spectra of digested **$(NH_2)_{100}$-MOF-508** in DMSO-d^{6}

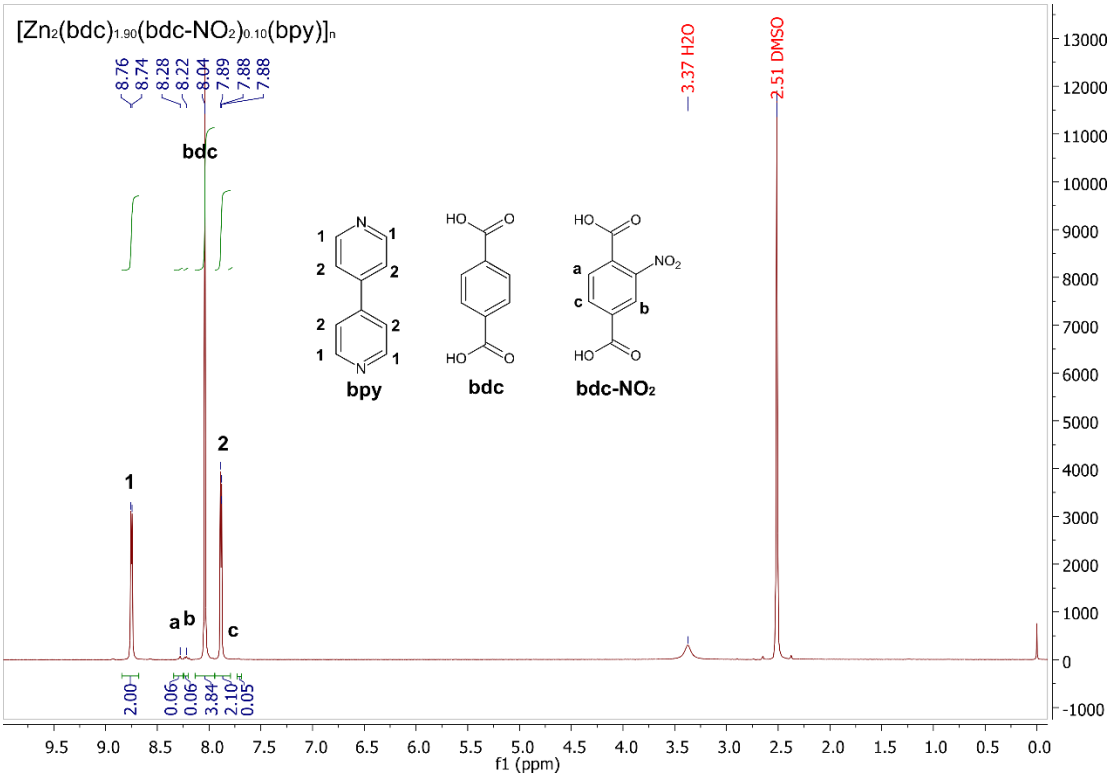

Supplementary **Figure 9** | ^{1}H-NMR spectra of digested **$(NO_2)_5$-MOF-508** in DMSO-d^{6}

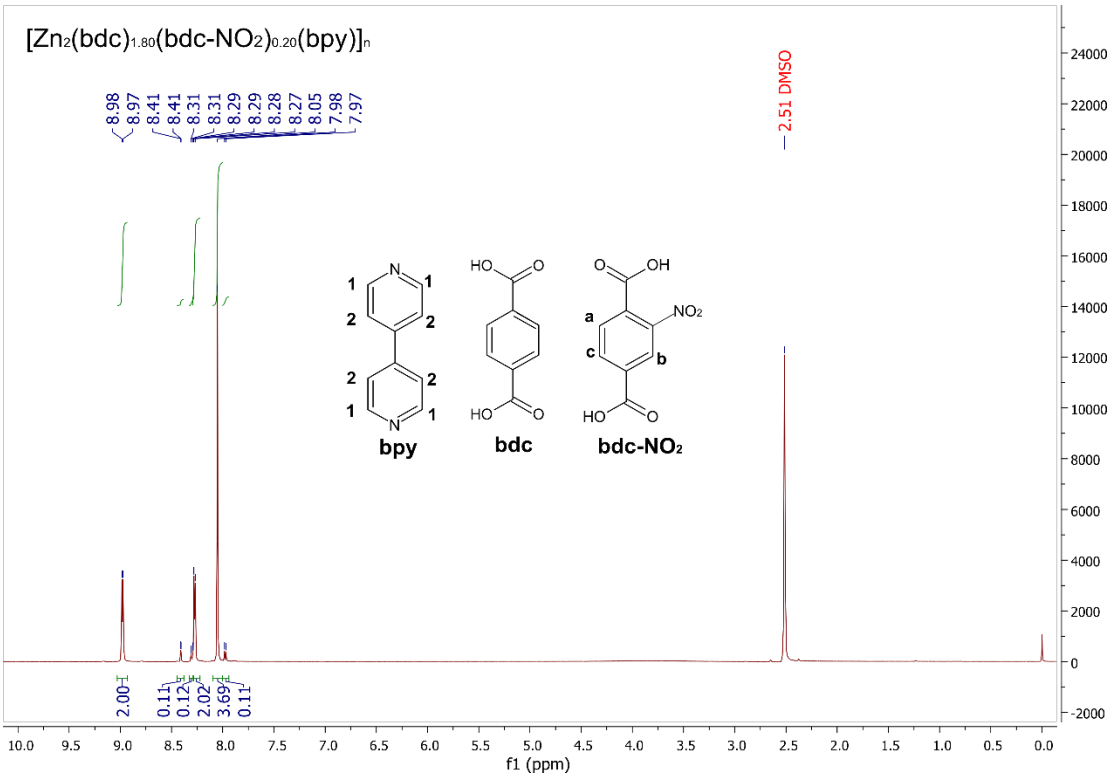

Supplementary **Figure 10 |** ^{1}H-NMR spectra of digested **$(NO_2)_{10}$-MOF-508** in DMSO-d^{6}

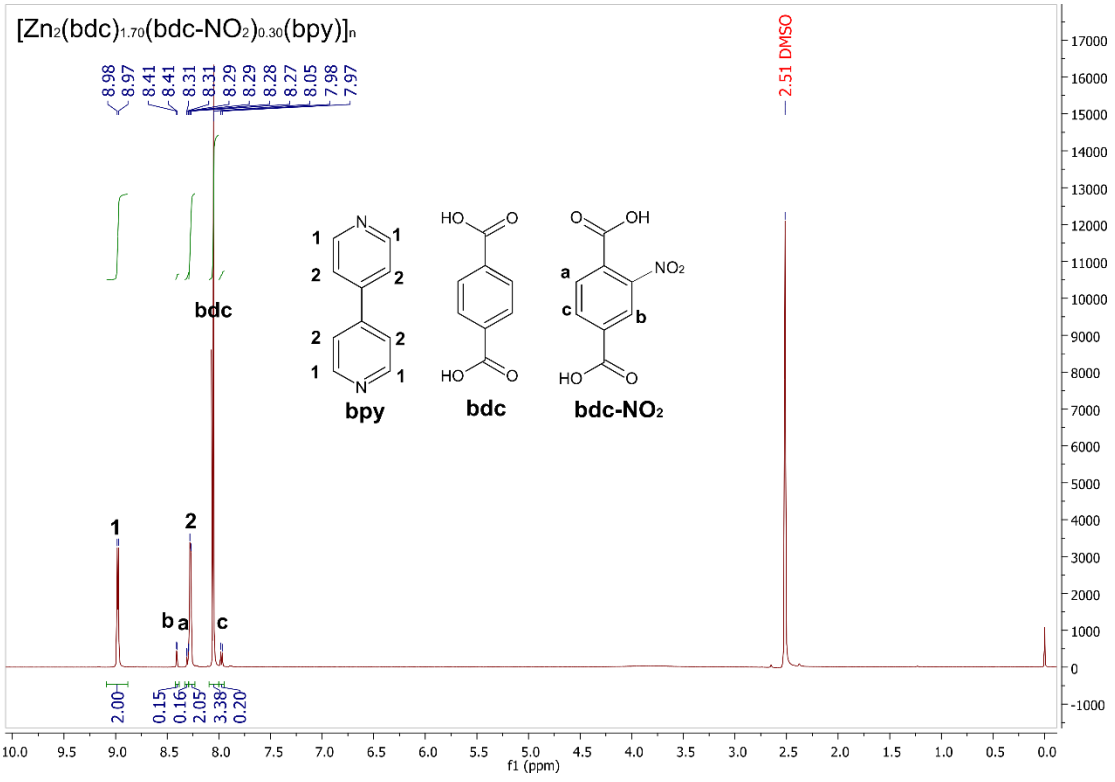

Supplementary **Figure 11 |** ^{1}H-NMR spectra of digested **$(NO_2)_{15}$-MOF-508** in DMSO-d^{6}

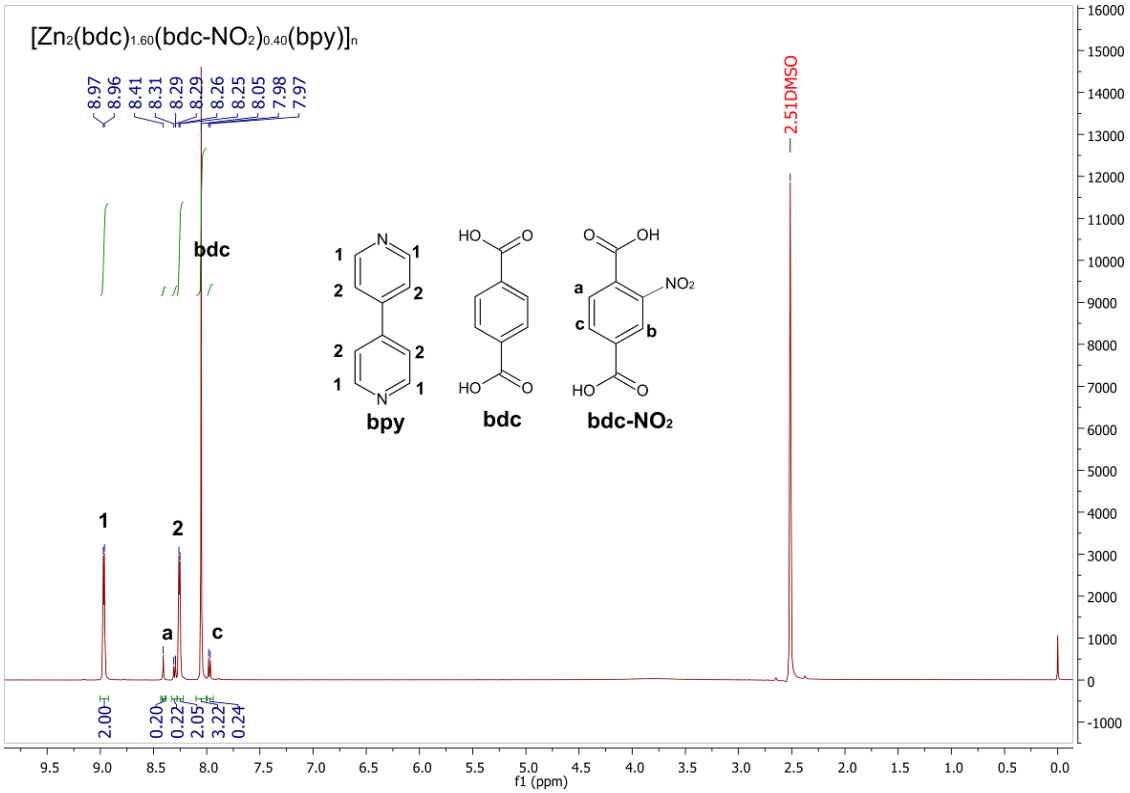

Supplementary **Figure 12 |** ^{1}H-NMR spectra of digested **$(NO_2)_{20}$-MOF-508** in DMSO-d^{6}

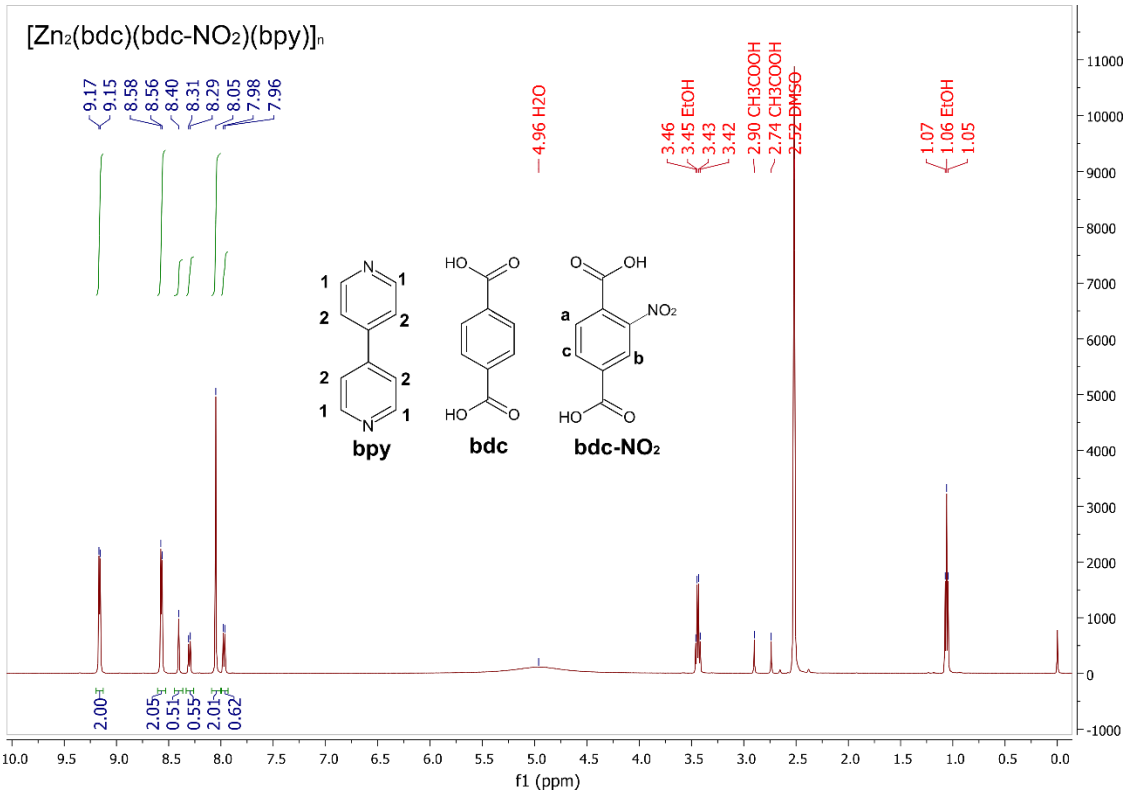

Supplementary **Figure 13 |** ^{1}H-NMR spectra of digested **$(NO_2)_{50}$-MOF-508** in DMSO-d^{6}

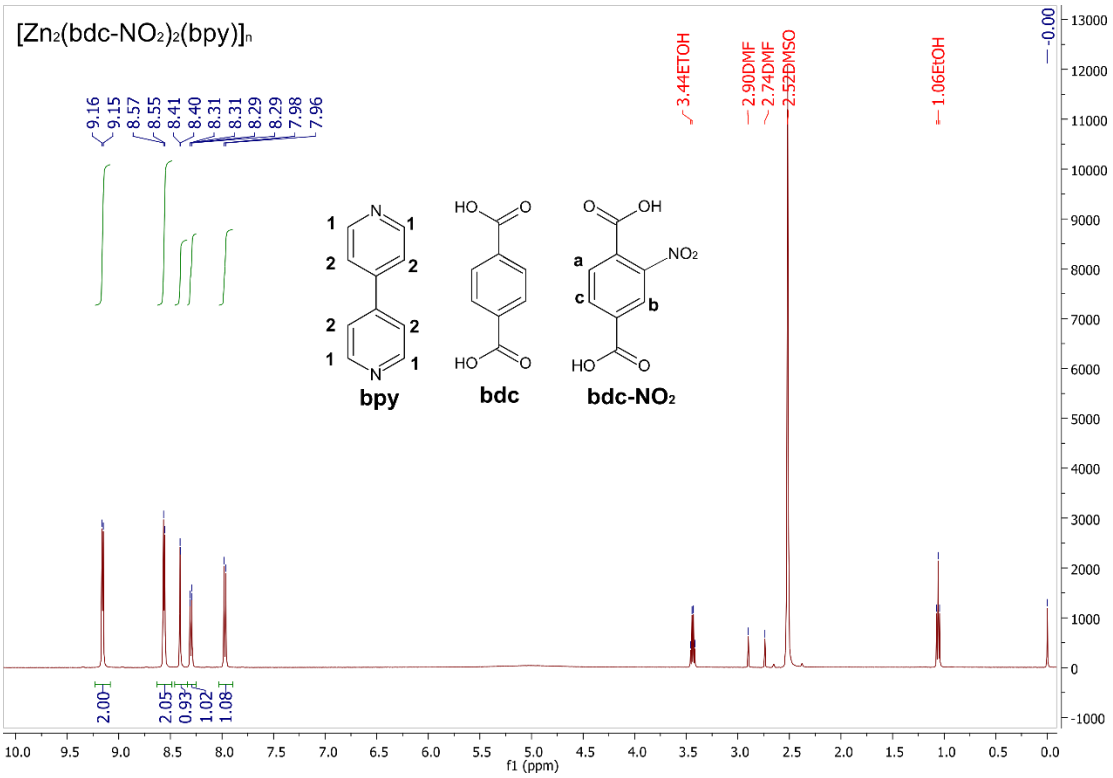

Supplementary **Figure 14 |** ^{1}H-NMR spectra of digested **$(NO_2)_{100}$-MOF-508** in DMSO-d^{6}

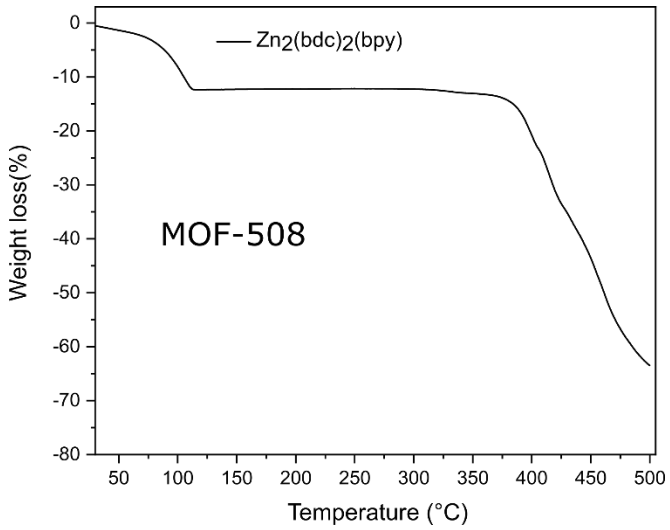

Supplementary **Figure 15.** Thermogravimetric analysis from 30 °C to 500 °C of **MOF-508** under nitrogen flow. The mass loss up to 400 °C is attributed to solvents, DMF and EtOH followed by material decomposition.

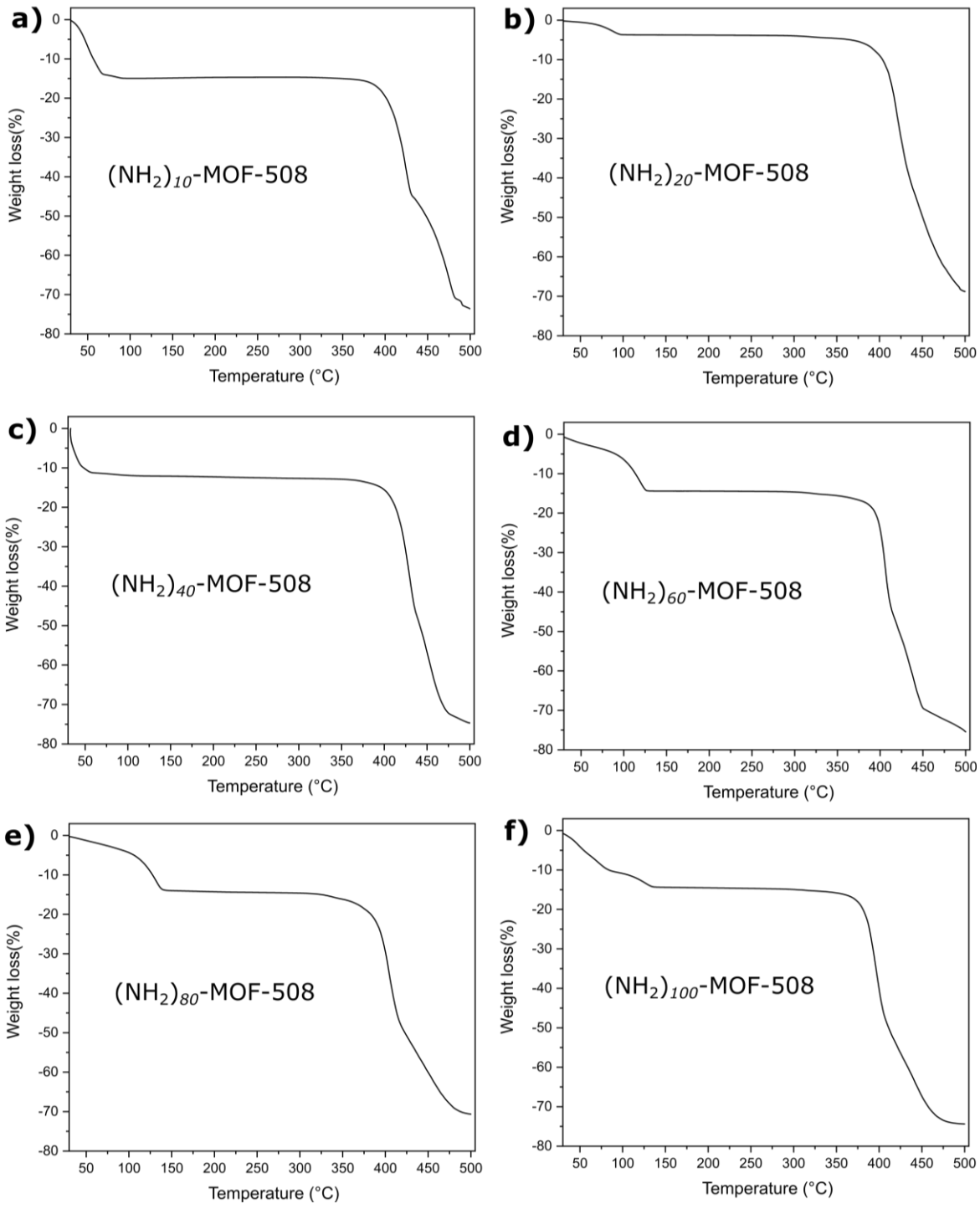

Supplementary **Figure 16.** Thermogravimetric analysis from 30 °C to 500 °C of **$(NH_2)_n$-MOF-508** under nitrogen flow. The mass loss up to 400 °C is attributed to solvents, DMF and EtOH followed by material decomposition.

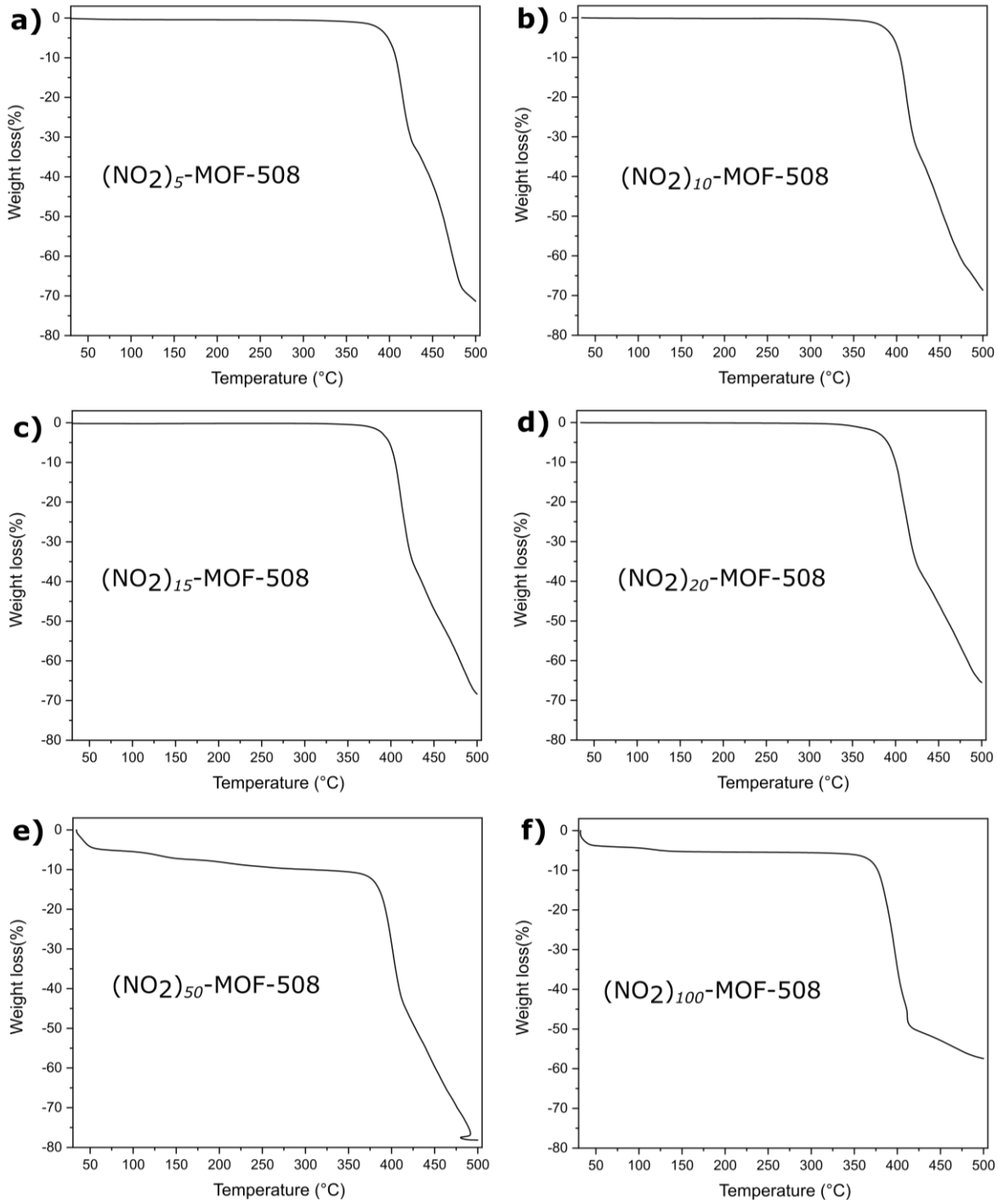

Supplementary **Figure 17.** Thermogravimetric analysis from 30 °C to 500 °C of **$(NO_2)_n$-MOF-508** under nitrogen flow. The mass loss up to 400 °C is attributed to solvents, DMF and EtOH followed by material decomposition.

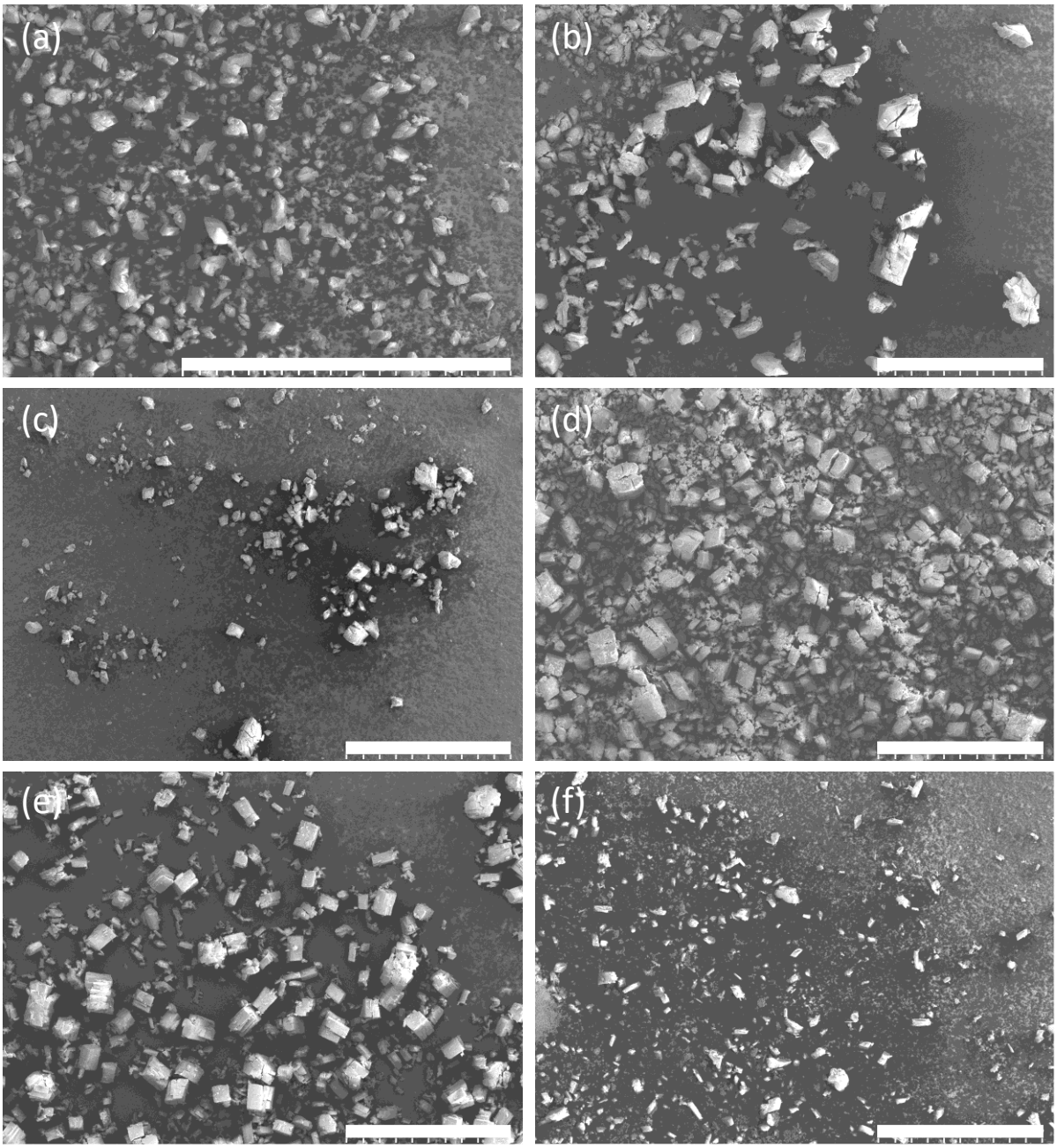

Supplementary **Figure 18.** Scanning electron microscopy images (scale 200 μm) of as synthesized **$(NH_2)_n$-MOF-508** a) **$(NH_2)_5$-MOF-508**, b) **$(NH_2)_{10}$-MOF-508**, c) **$(NH_2)_{20}$-MOF-508**, d) **$(NH_2)_{40}$-MOF-508** e) **$(NH_2)_{60}$-MOF-508**, f) **$(NH_2)_{100}$-MOF-508**.

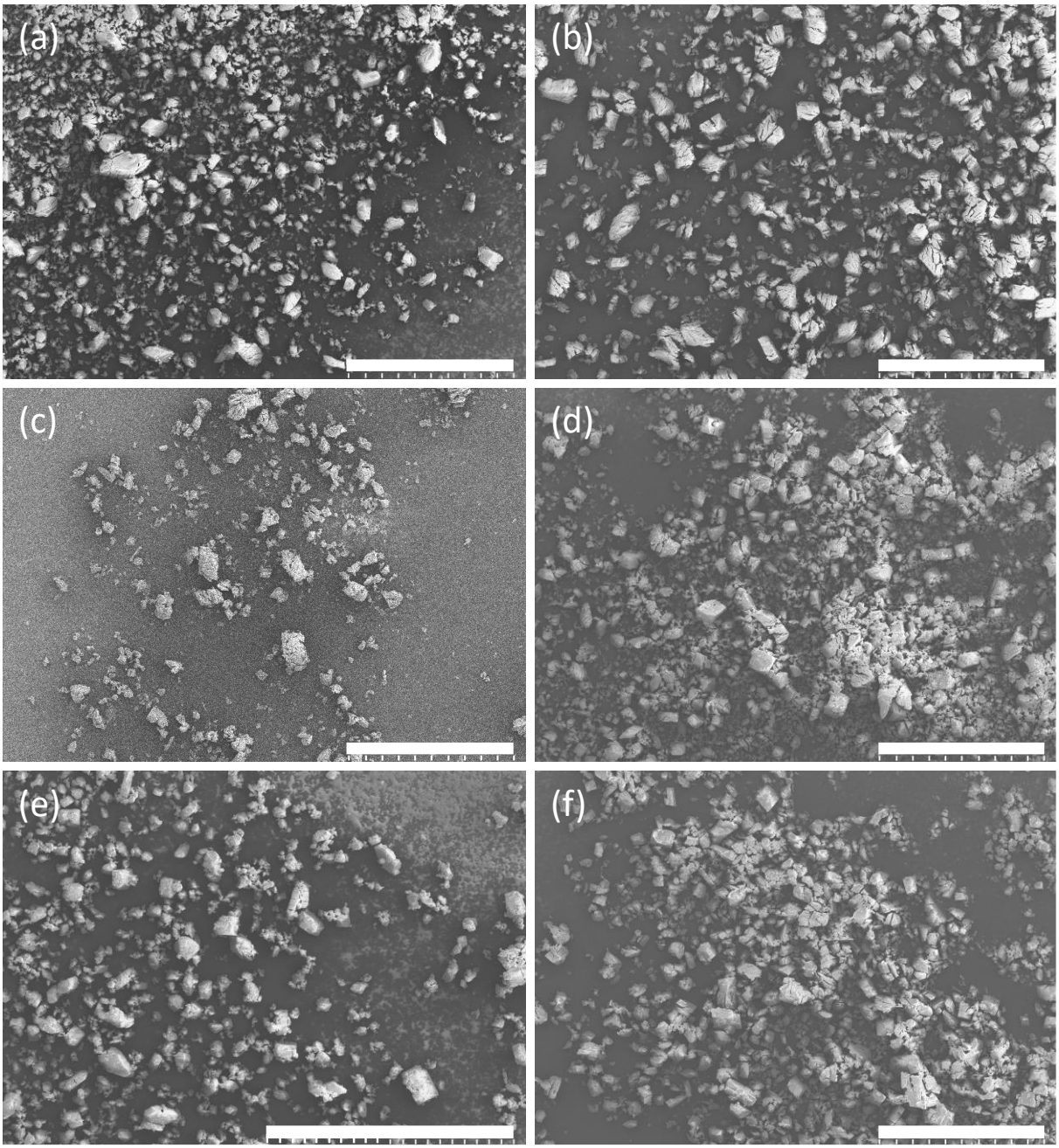

Supplementary **Figure 19.** Scanning electron microscopy images (scale 200 μm) of as synthesized **$(NO_2)_n$-MOF-508** a) **$(NO_2)_5$-MOF-508**, b) **$(NO_2)_{10}$-MOF-508**, c) **$(NO_2)_{15}$-MOF-508**, d) **$(NO_2)_{20}$-MOF-508**, e) **$(NO_2)_{50}$-MOF-508**, f) **$(NO_2)_{100}$-MOF-508**.

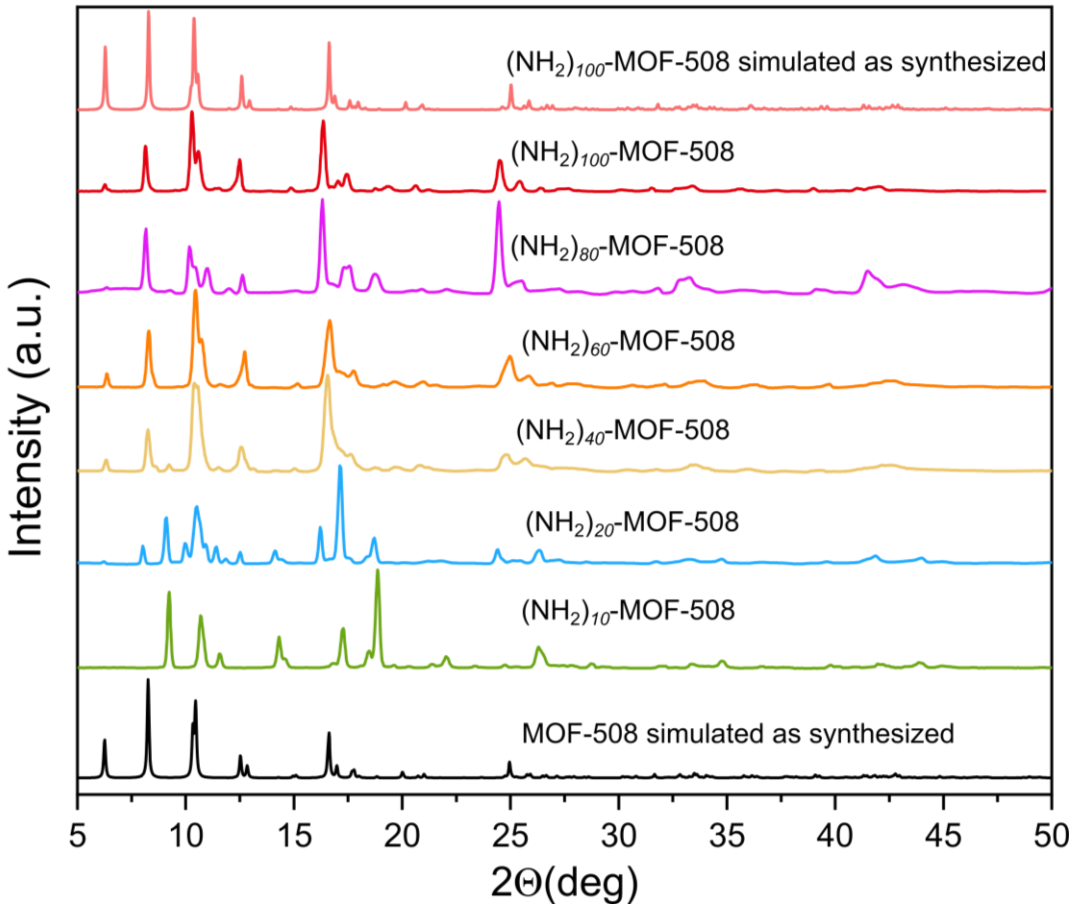

Supplementary **Figure 20.** Powder X-Ray diffraction patterns of as-synthesized **$(NH_2)_n$-MOF-508**. The experimental patterns are compared to the simulated pattern based on the refined **MOF-508a** and **$(NH_2)_{100}$-MOF-508** single crystal structures.

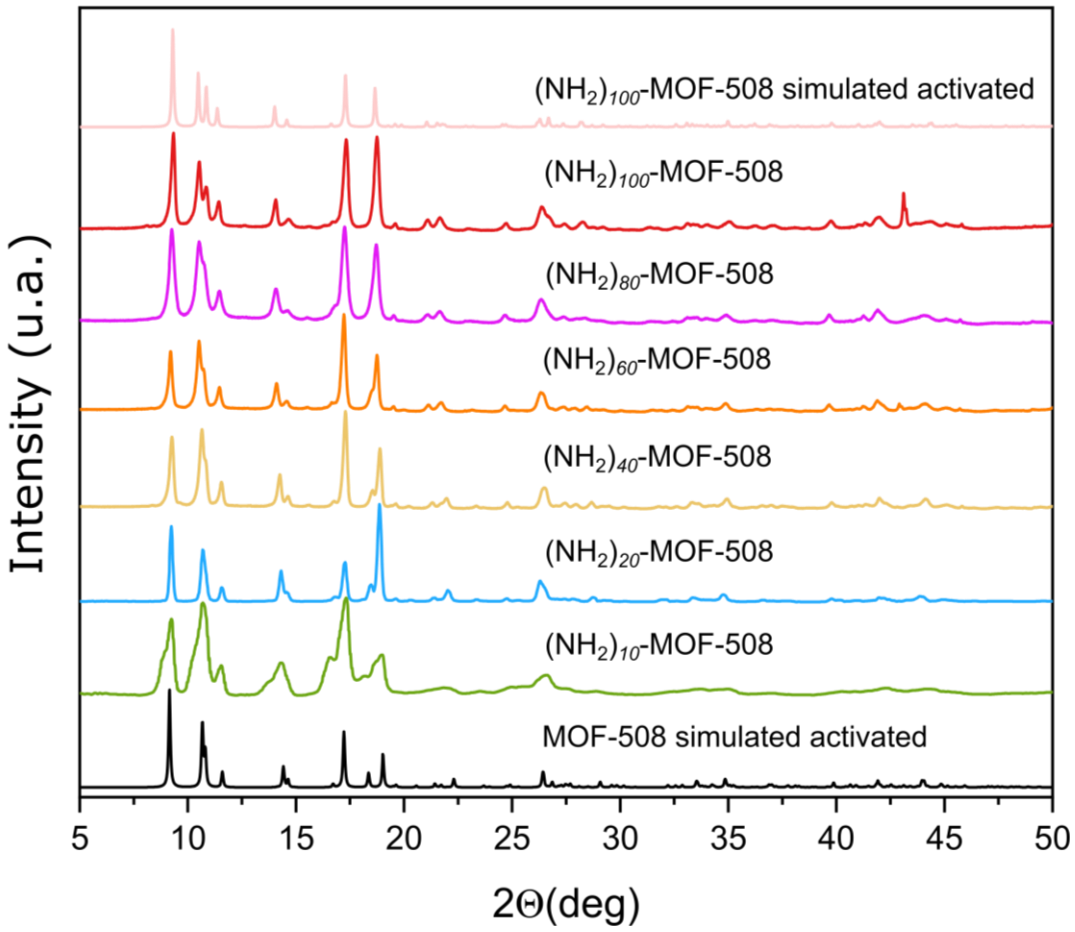

Supplementary **Figure 21.** Powder X-Ray diffraction patterns of activated **$(NH_2)_n$-MOF-508**. The experimental patterns are compared to the simulated pattern based on the refined **MOF-508b** and **$(NH_2)_{100}$-MOF-508** single crystal structures.

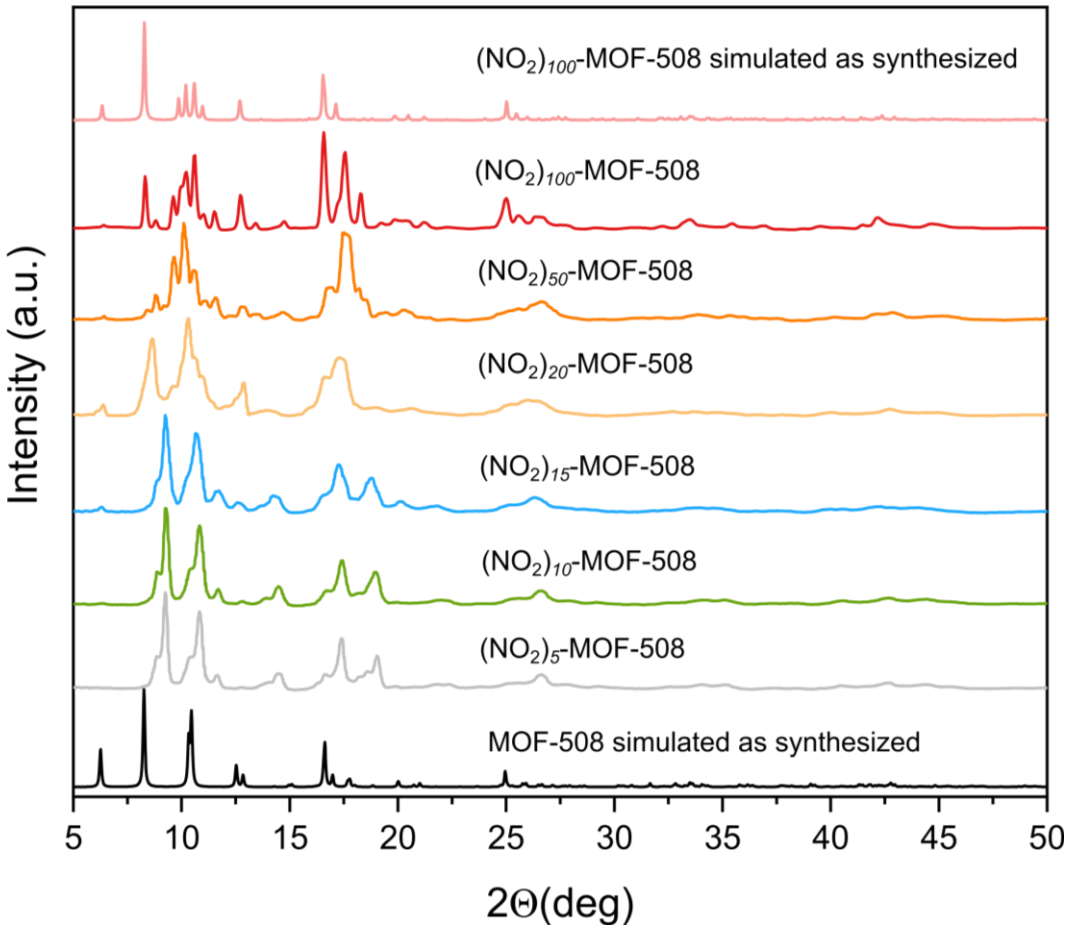

Supplementary **Figure 22.** Powder X-Ray diffraction patterns of as-synthesized **$(NO_2)_n$-MOF-508**. The experimental patterns are compared to the simulated pattern based on the refined **MOF-508a** and **$(NO_2)_{100}$-MOF-508** single crystal structures.

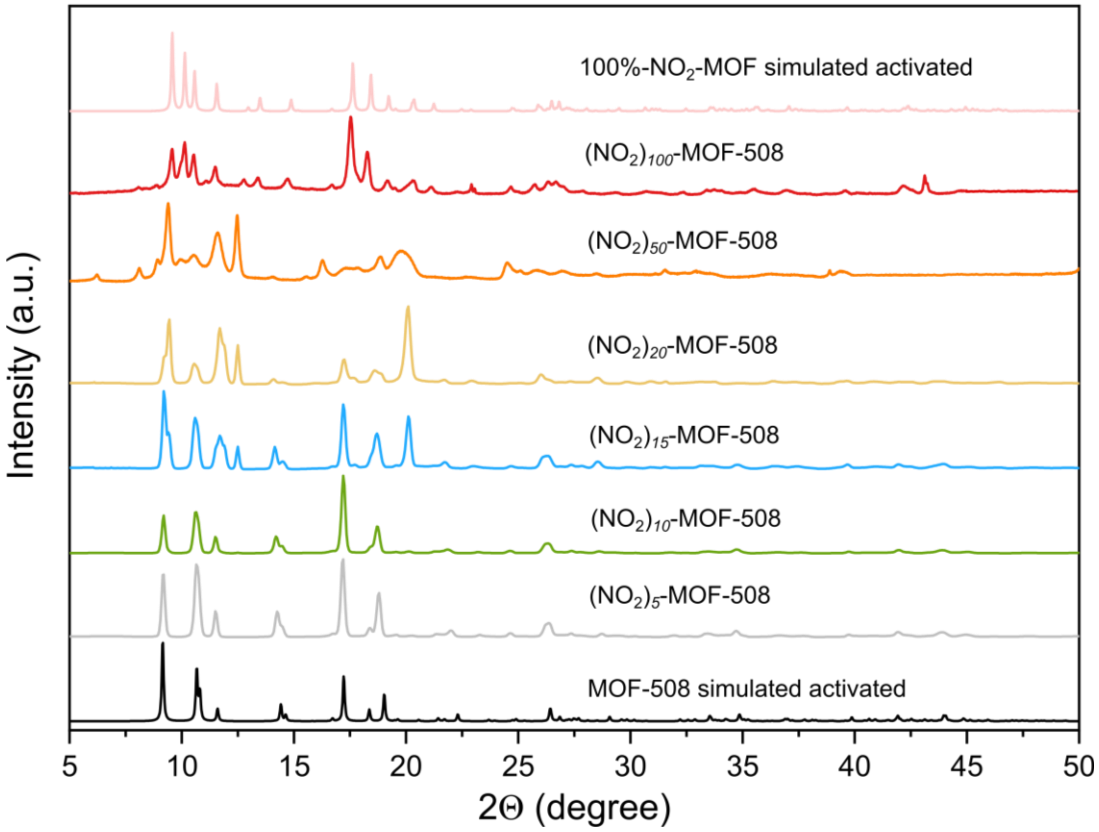

Supplementary **Figure 23.** Powder X-Ray diffraction patterns of activated **$(NO_2)_n$-MOF-508**. The experimental patterns are compared to the simulated pattern based on the refined **MOF-508b** and **$(NO_2)_{100}$-MOF-508** single crystal structures.

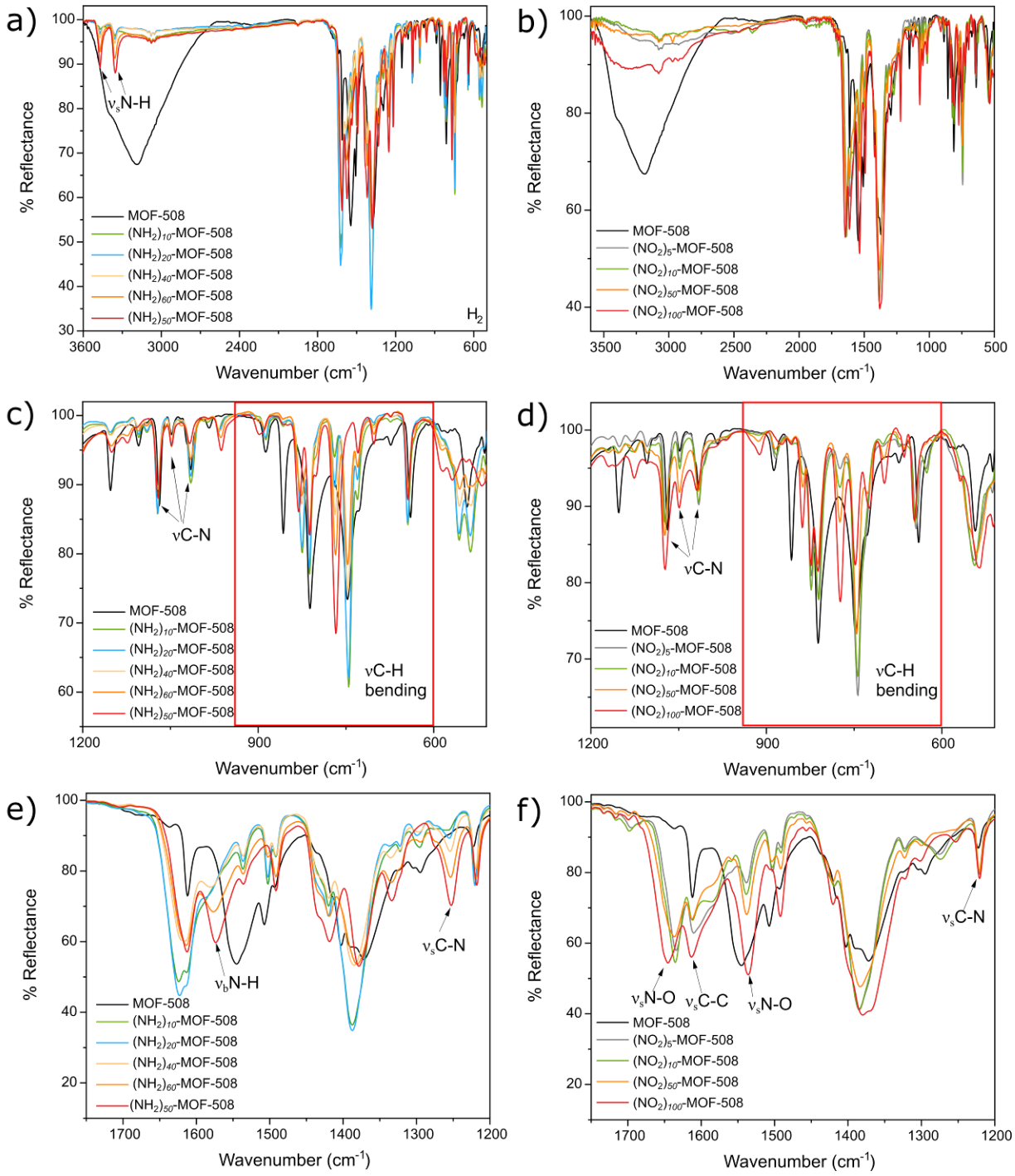

Supplementary **Figure 24.** Infrared analysis of **$(NH_2)_n$-MOF-508** and **$(NH_2)_n$-MOF-508** The reference **MOF-508** was added for comparison.

UV-vis analysis:

bdc-X functional groups influence the conjugation of the system, leading to a shift of the absorption peak, in the UV-vis spectra, to the higher wavelength compared to the non-functional **MOF-508**. The UV spectra of **MOF-508**, **$(NH_2)_n$-MOF-508** and **$(NO_2)_n$-MOF-508** materials show that **MOF-508** has a unique absorption band at λ = 275 nm whereas ***n%*-NO_2-MOF** show one additional band at λ = 350 nm for **$(NO_2)_{10}$-MOF-508** and three additional band at λ = 350 nm, λ = 425 nm and 540 nm for **$(NH_2)_{100}$-MOF-508**. **$(NH_2)_n$-MOF-508** shows an additional absorption band at λ = 380 nm compared to **MOF-508**. These results indicate a more conjugated system for **$(NH_2)_n$-MOF-508** and **$(NO_2)_n$-MOF-508** compared to **MOF-508**.

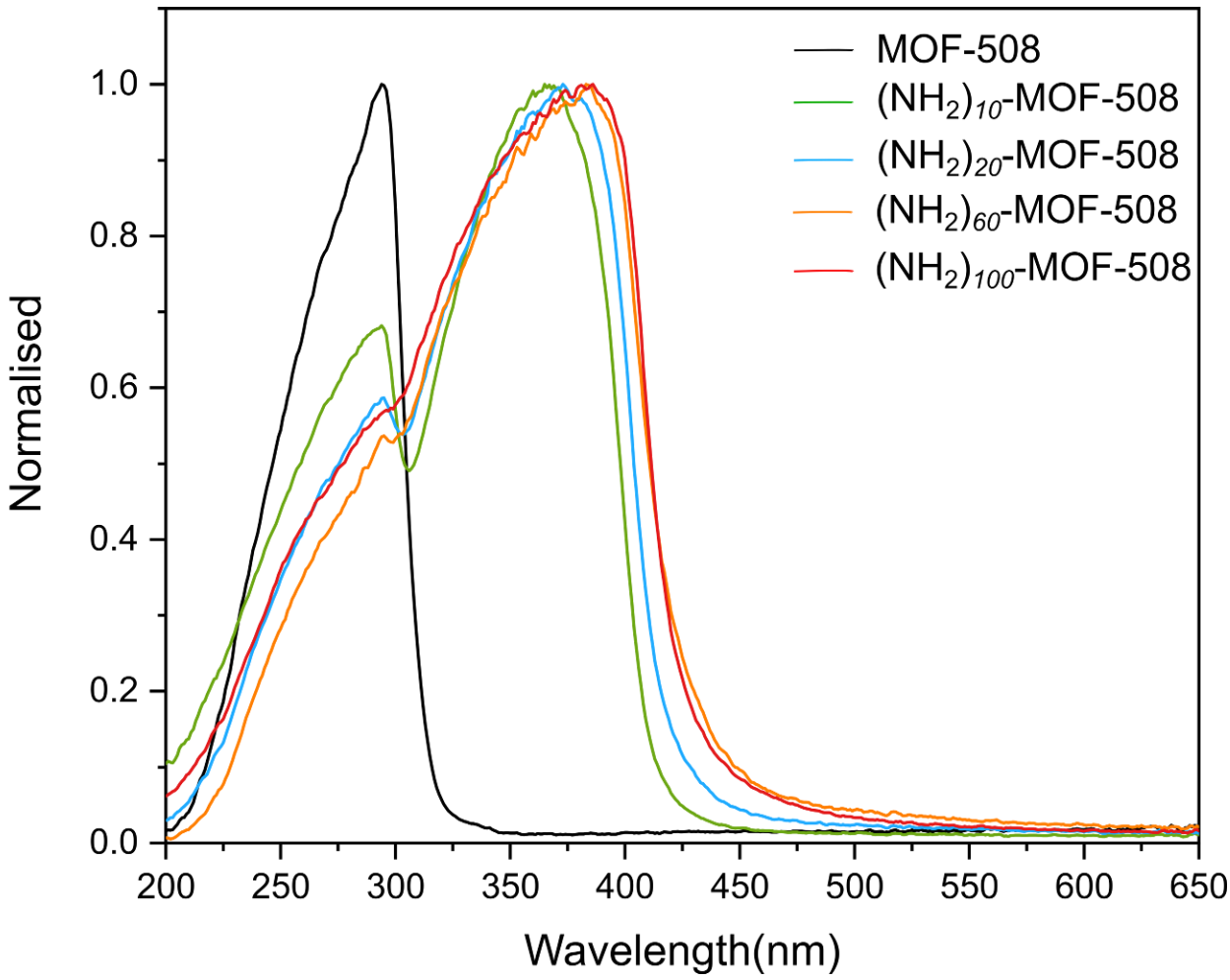

Supplementary **Figure 25.** UV-visible of **$(NH_2)_n$-MOF-508**. The reference **MOF-508** was added for comparison

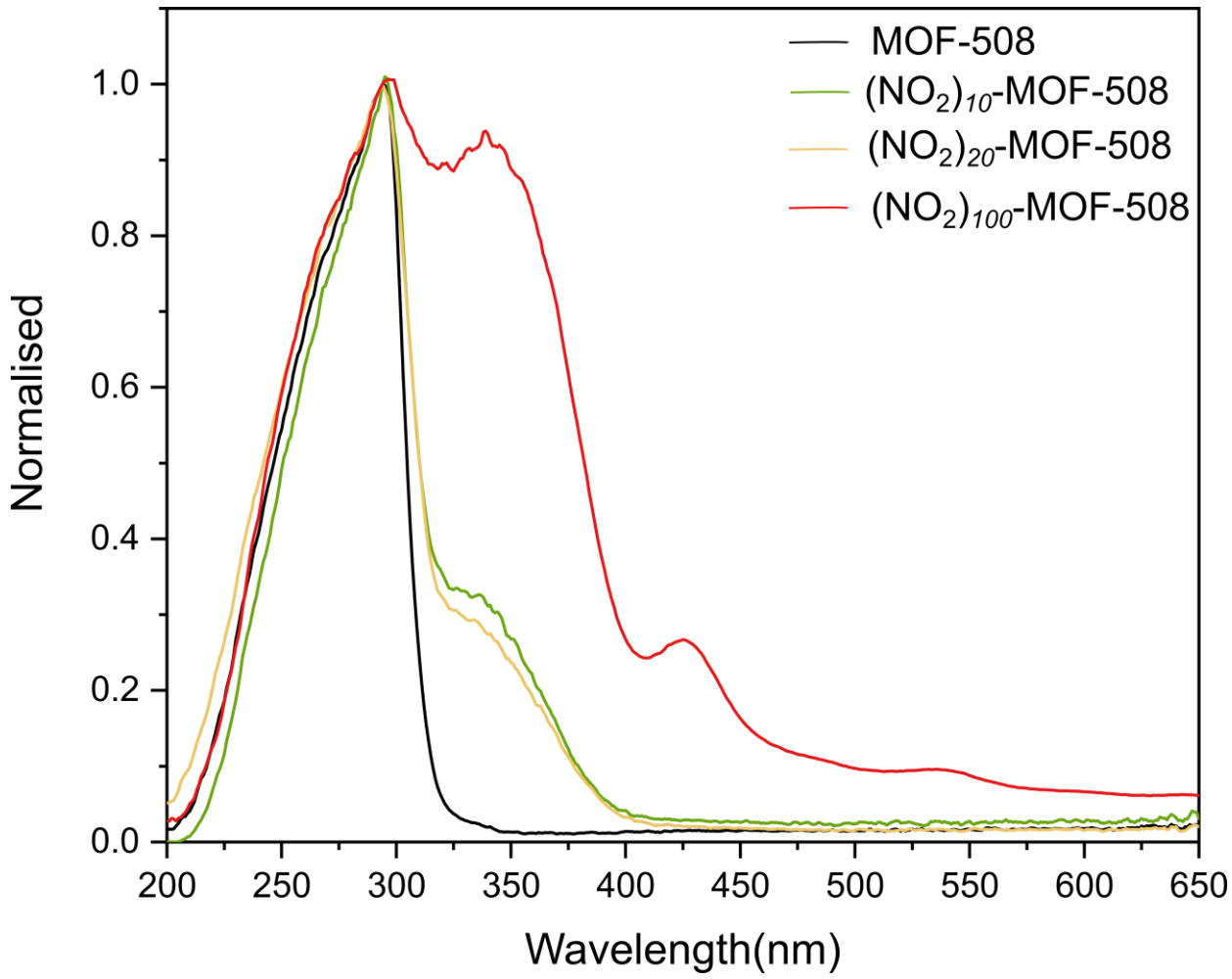

Supplementary **Figure 26.** UV-visible of **$(NO_2)_n$-MOF-508**. The reference **MOF-508** was added for comparison

Supplementary **Table 1.** Crystallographic details on collapsed **MOF-508** series

	$(NH_2)_{100}$-MOF-508 collapsed	**MOF-508b** collapsed	**$(NO_2)_{100}$-MOF-508** collapsed
CCDC identifier	YUDTAV	ETIPEE	
Deposition number	1986606	1429432	
Formula	$C_{26}H_{16}N_4O_8Zn_2$	$C_{26}H_{12}N_2O_8Zn_2$	$C_{26}H_{12}N_4O_{12}Zn_2$
a (Å)	8.02114(26)	7.9917(13)	8.0536(13)
b (Å)	9.49877(33)	9.4227(16)	10.1473(17)
c (Å)	10.8389(4)	10.5835(17)	10.2709(17)
α	61.1965(16)	65.314(2)	63.945(4)
β	82.4131(31)	86.464(2)	83.150(6)
γ	75.9782(23)	86.464(2)	71.754(5)
Space group	P 1	P 1	P 1
Crystal system	Triclinic	Triclinic	Triclinic
V ($Å^3$)	701.977	703.59	715.982
Z	1	1	1
T (K)	293K	298K	195K
λ (Å)	0.799671(1)		0.41270
R factor	5.55	5.88	8.81
Crystal density ($g.cm^{-3}$)	1.53	1.45	1.63
Reference	10.1002/ange.202003186	10.1039/C6CC06709C	This work

Supplementary **Table 2.** Crystallographic details on as-synthesized **MOF-508** series

	$(NH_2)_{100}$-MOF-508 as-synthesized	**MOF-508b** as-synthesized	**MOF-508b** filled with CO_2	**$(NO_2)_{100}$-MOF-508** as-synthesized
CCDC identifier	YUDTUP	ECIWUJ01	ETIPII	
Deposition number	1970820	1429431	1429433	
Formula	$C_{26}H_{18}N_4O_8Zn_2$ 0.5(DMF)	$C_{26}H_{16}N_2O_8Zn_2$	$C_{26}H_{16}N_2O_8Zn_2$	$C_{26}H_{12}N_4O_{12}Zn_2$
a (Å)	10.9150(7)	10.887(5)	14.099(10)	10.9023(3)
b (Å)	10.9302(7)	10.896(4)	10.997(8)	10.9089(3)
c (Å)	14.0601(4)	14.070(6)	21.865(15)	14.0384(3)
α	88.112(3)	91.252(4)	90.00	95.951(2)
β	89.710(4)	92.588(5)	93.971(9)	91.201(2)
γ	77.463(5)	104.430(5)	90.00	100.414(2)
Space group	P 1	P 1	P $2_1/c$	P 1
Crystal system	Triclinic	Triclinic	Triclinic	Triclinic
V ($Å^3$)	1636.53	1613.80	3381.96	1631.92
Z	2	2	4	2
T (K)	100	298	253	298
λ (Å)	0.71073			
R factor	12.34	8.62	8.77	7.52
Crystal density ($g.cm^{-3}$)	1.38	1.27	1.28	1.41
References	10.1002/ange.202003186	10.1039/C6CC06709C	10.1039/C6CC06709C	This work

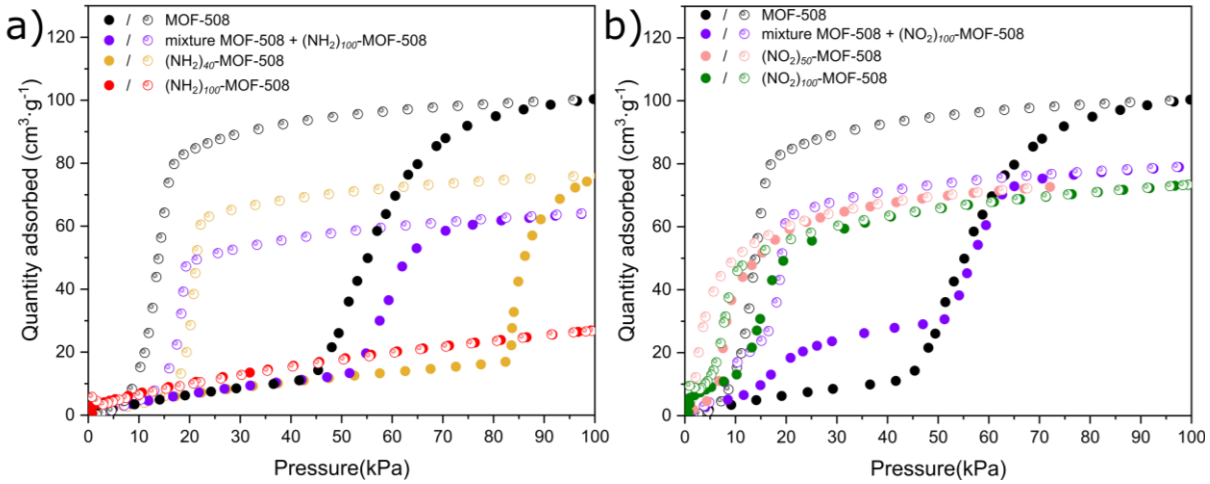

Supplementary **Figure 27.** Acetylene (C_2H_2) adsorption (filled symbols)/desorption (empty symbols) isotherms at 273 K for a) mixture of **MOF-508** and **$(NH_2)_{100}$-MOF-508** (in a ratio 6:4) b). mixture of **MOF-508** and **$(NO_2)_{100}$-MOF-508** (in a ratio 1:1). **MOF-508**, **$(NH_2)_{100}$-MOF-508**, **$(NO_2)_{100}$-MOF-508**, **$(NH_2)_{60}$-MOF-508** and **$(NO_2)_{50}$-MOF-508** isotherms were added for comparison.

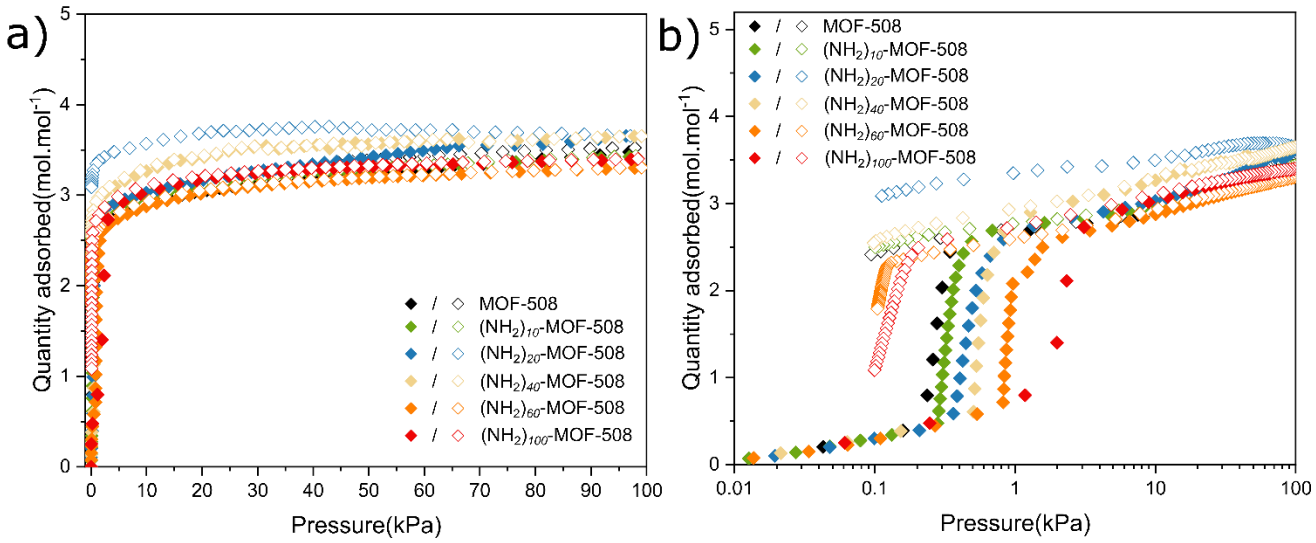

Supplementary **Figure 28.** Acetylene (C_2H_2) adsorption (filled symbols)/desorption (empty symbols) isotherms for **$(NH_2)_n$-MOF-508** at 195 K. **MOF-508** isotherm was added for comparison.

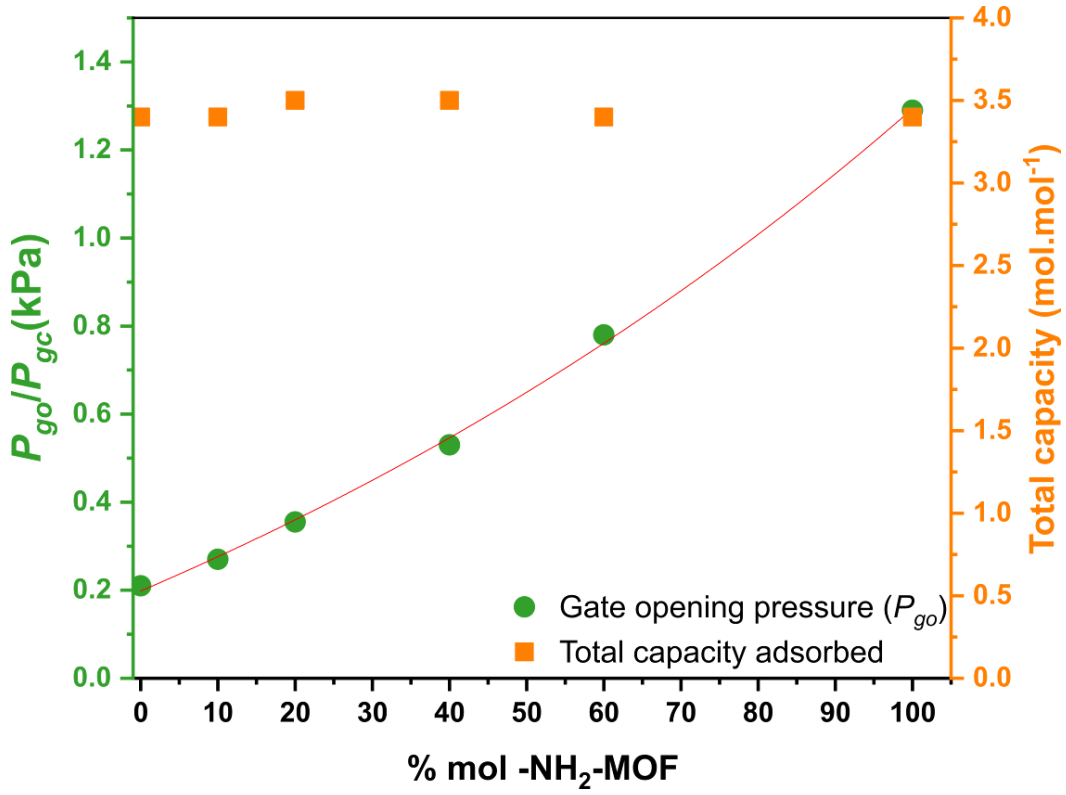

Supplementary **Figure 29.** Gate opening pressures and total capacities of **$(NH_2)_n$-MOF-508** for acetylene (C_2H_2) at 195 K. **MOF-508** isotherm was added for comparison.

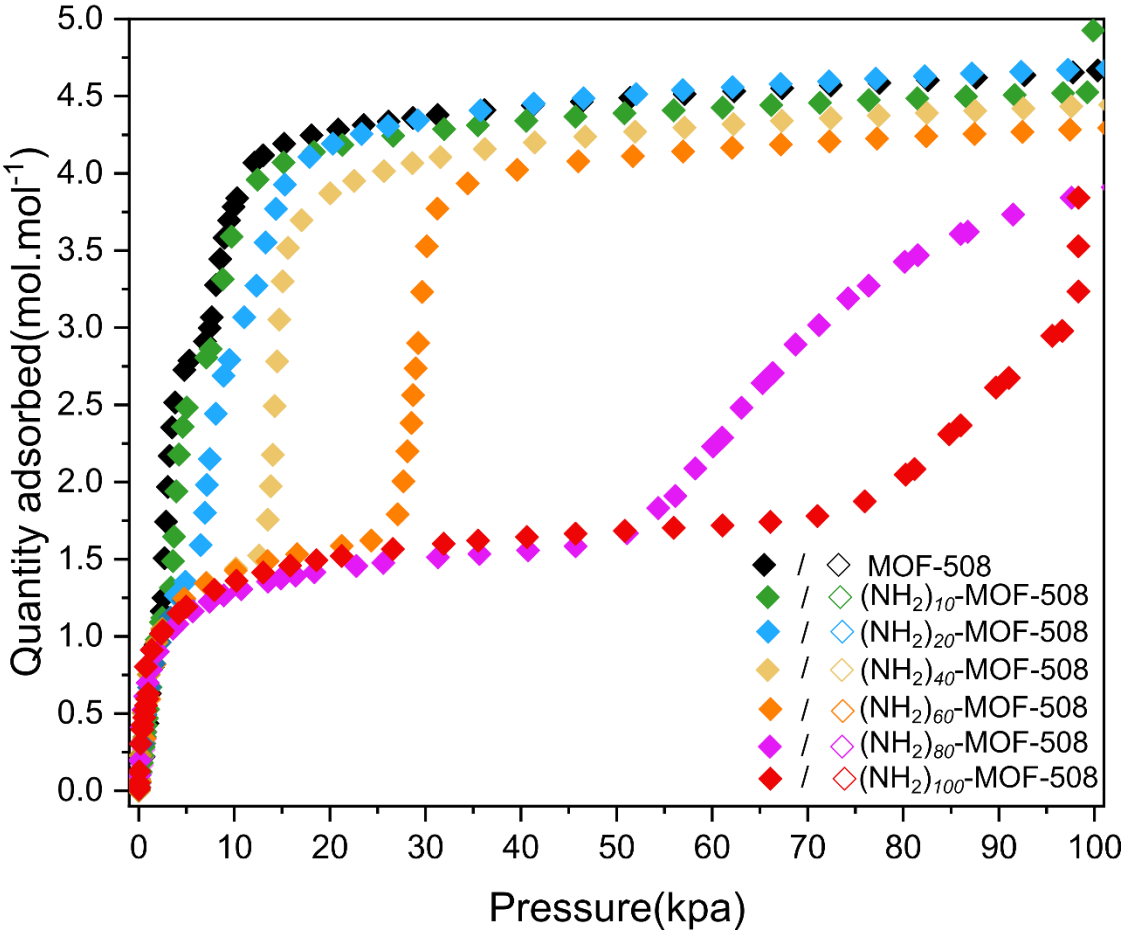

Supplementary **Figure 30.** Carbon dioxide (CO_2) adsorption isotherms for **$(NH_2)_n$-MOF-508** at 195 K. **MOF-508** isotherm was added for comparison.

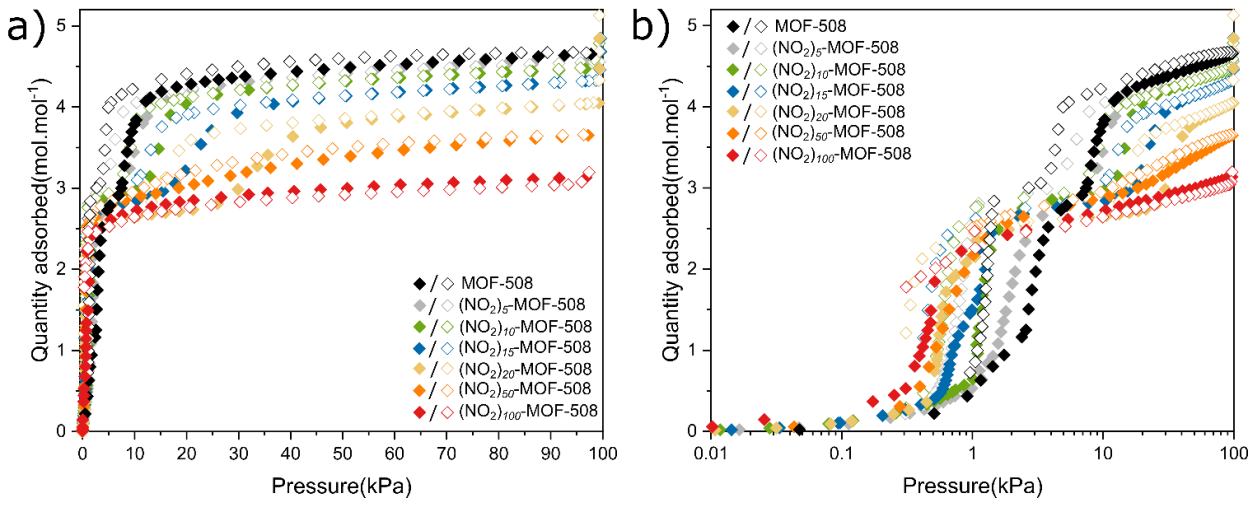

Supplementary **Figure 31.** Carbon dioxide (CO_2) adsorption (filled symbols)/desorption (empty symbols) isotherms for **$(NO_2)_n$-MOF-508** at 195 K. **MOF-508** isotherm was added for comparison.

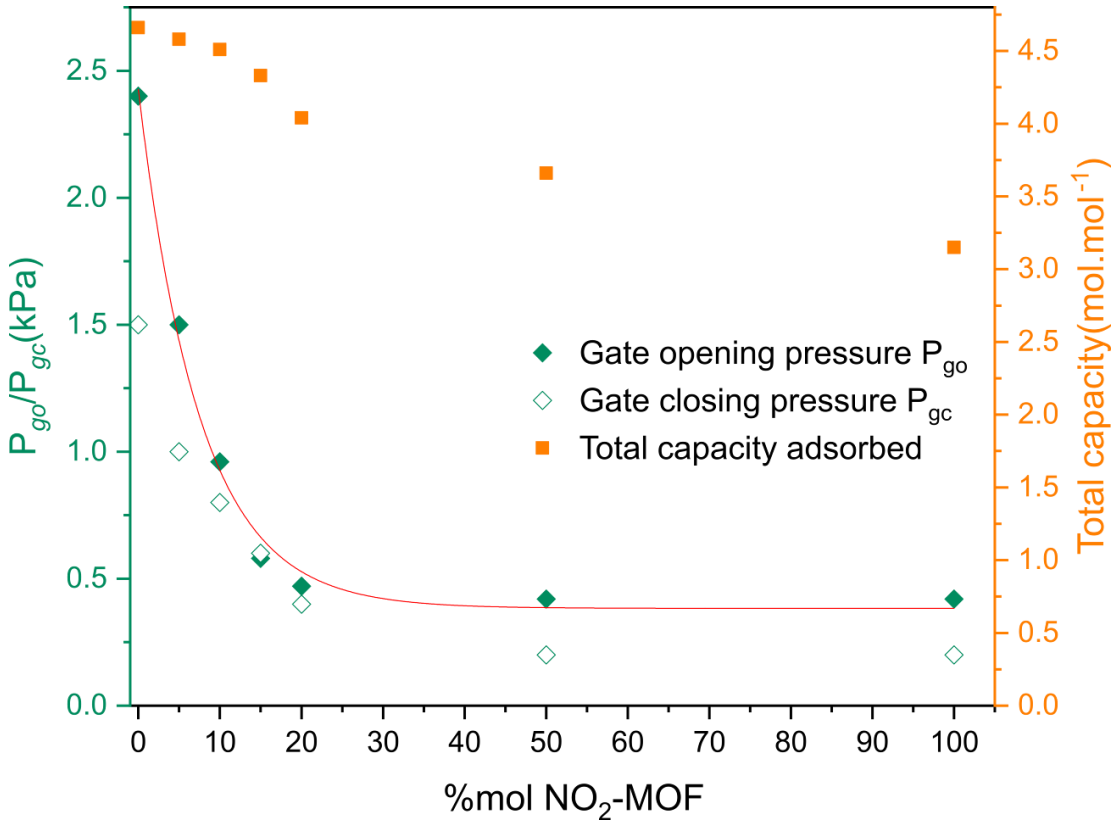

Supplementary **Figure 32.** Gate opening pressures and total capacities of **$(NO_2)_n$-MOF-508** for carbon dioxide (CO_2) at 195K. **MOF-508** isotherm was added for comparison.

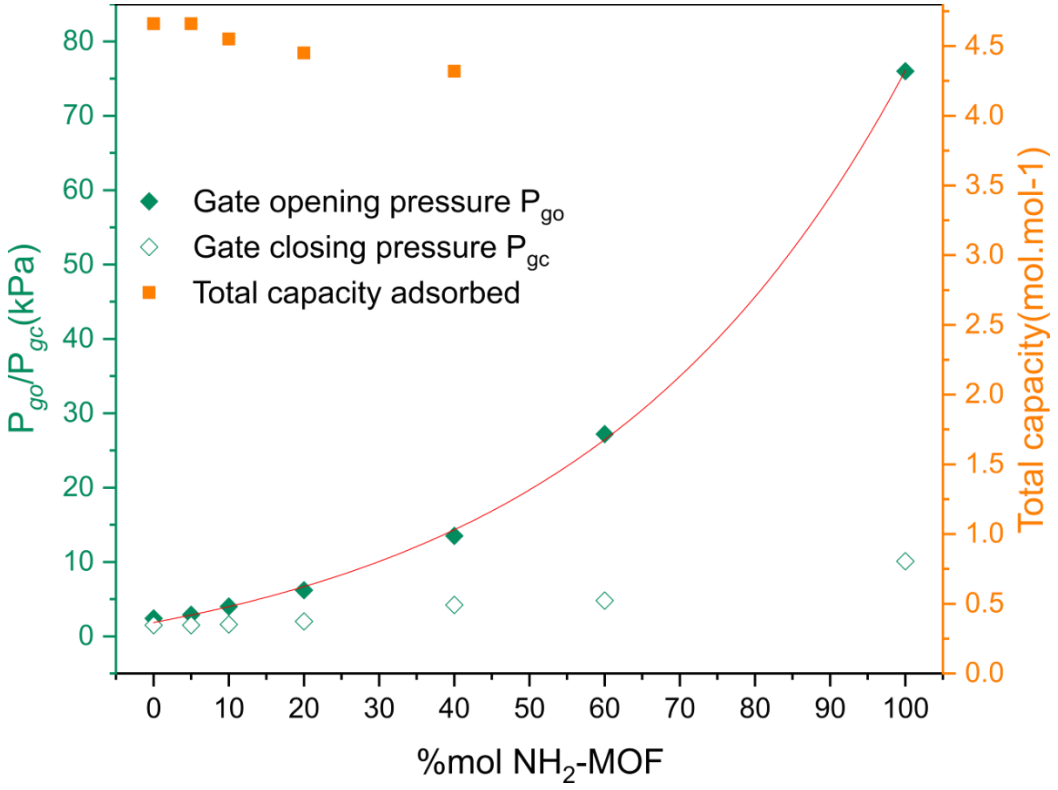

Supplementary **Figure 33.** Gate opening pressures and total capacities of **$(NH_2)_n$-MOF-508** for carbon dioxide (CO_2) at 195K. **MOF-508** isotherm was added for comparison.

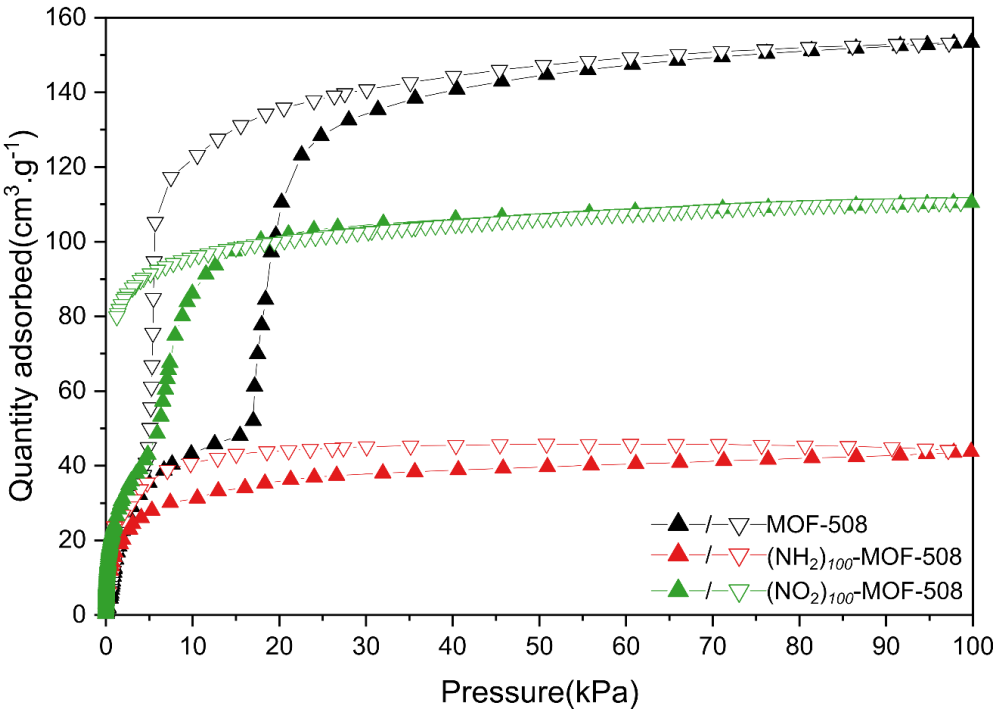

Supplementary **Figure 34.** Methane (CH_4) adsorption (filled symbols)/desorption (empty symbols) isotherms for **MOF-508**, **$(NH_2)_{100}$-MOF-508** and **$(NO_2)_{100}$-MOF-508** at 150K.

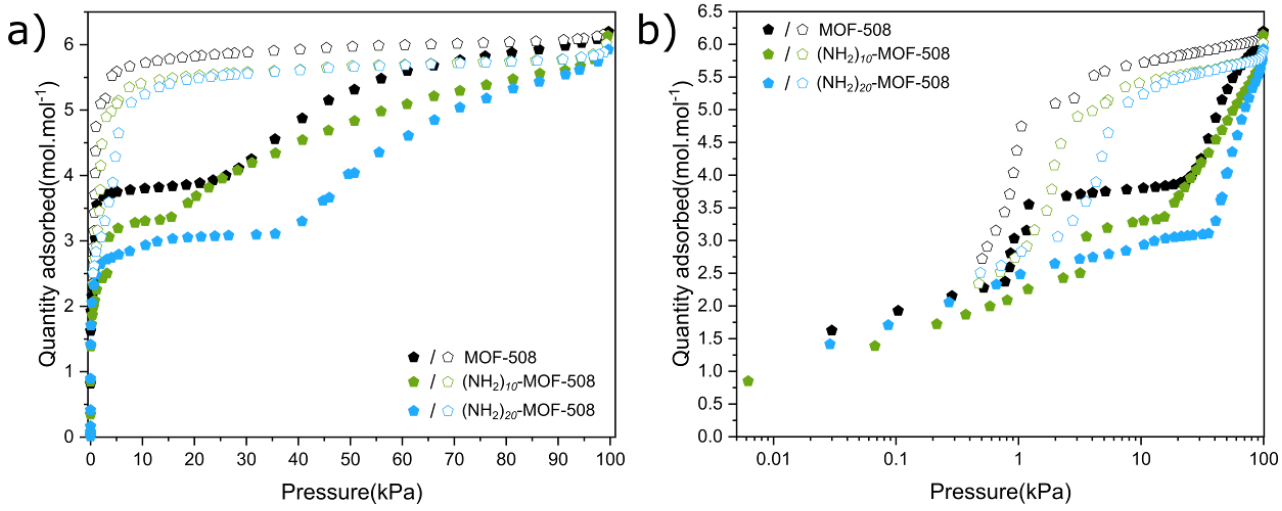

Supplementary **Figure 35.** Oxygen (O_2) adsorption (filled symbols)/desorption (empty symbols) isotherms for **$(NH_2)_n$-MOF-508** at 90 K. **MOF-508** isotherm was added for comparison.

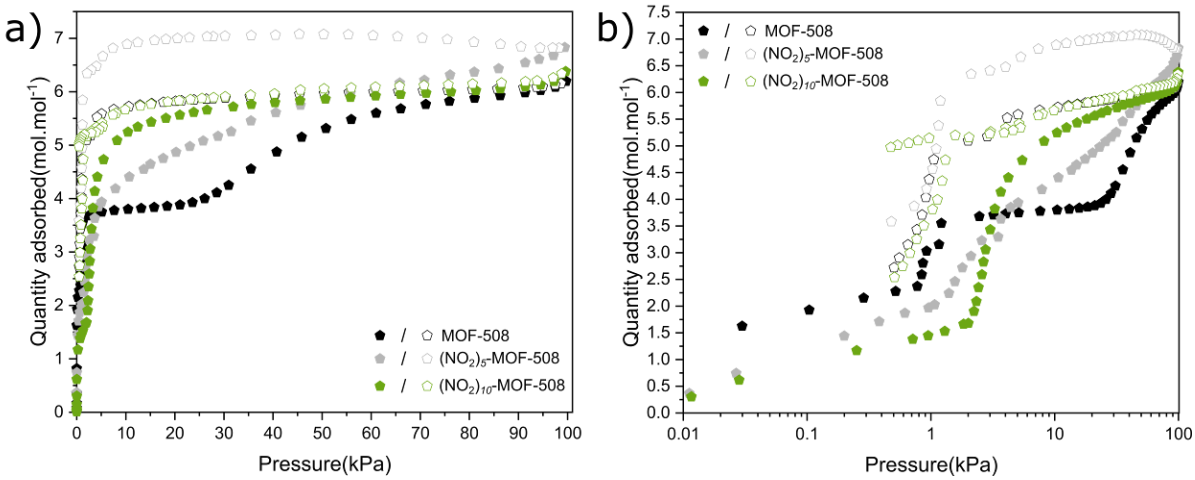

Supplementary **Figure 36.** Oxygen (O_2) adsorption (filled symbols)/desorption (empty symbols) isotherms for **$(NO_2)_n$-MOF-508** at 90 K. **MOF-508** isotherm was added for comparison.

Description of the thermodynamic model in the osmotic ensemble

Thermodynamic stability of flexible porous materials, where the host framework undergoes structural phase transitions induced by the adsorption of a fluid, are appropriately described in the osmotic statistical ensemble, where the thermodynamic potential Ω_{os} is written as:[1]

$$\Omega_{os} = U - TS - \mu_{ads} N_{ads} + PV$$

For an multistable adsorbent framework, the thermodynamic potential of each phase *i* is then given by $\Omega_{os}^{i}(T, P)$, which can be written as:[2]

$$\Omega_{os}^{i}(T,P) = F_{host}^{i}(T) + PV_i - \int_0^P N_{ads}^{i}(\boldsymbol{p},\boldsymbol{T})\, \boldsymbol{V_m}(\boldsymbol{p},\boldsymbol{T})\, \boldsymbol{dp}$$

where $F_{host}^{i}(T)$ is the free energy of the phase, V_i its volume, $N_{ads}^{i}(\boldsymbol{p},\boldsymbol{T})$ is the "rigid host" adsorption isotherm in that phase, and $V_m(p,T)$ is the molar volume of the fluid. In the case of a

gate opening material, we consider an equilibrium between two phases (i = 1 or 2), with one nonporous phase ($N_{\text{ads}}^{1}(\boldsymbol{p},T) = \mathbf{0}$). Furthermore, in the case of an interpenetrated framework, both phases have the same unit cell volume, i.e., $V_1 = V_2$. All combined, we can write the osmotic potential difference between the two phases is:

$$\Delta\Omega_{\text{os}}(T,P) = \Delta F_{\text{host}}(T) - \int_0^P N_{\text{ads}}^{\text{open}}(\boldsymbol{p},\boldsymbol{T})\, \boldsymbol{V_m}(\boldsymbol{p},\boldsymbol{T})\, \boldsymbol{d}p$$

To go further in our analysis, we need to make an assumption about the nature of the adsorption process. Based on the validation of numerous previous work for adsorption of small molecules in metal–organic frameworks, we describe the "rigid host" isotherm in the open phase with a Langmuir-type isotherm:[3-4]

$$N_{\text{ads}}^{\text{open}}(P) = \frac{K\,P}{1+\frac{K\,P}{N}}$$

This isotherm has two parameters, the Henry constant K and the saturation uptake N. Finally, the molar volume V_m of the adsorbate in the gas phase is given by the ideal gas law.

Determination of thermodynamic model parameters

For a given triplet of (host material, adsorbate, temperature), we can determine the values of the thermodynamic parameters K and N by fitting the "open phase" adsorption. In order to do so, we fit the desorption branch of the isotherm, as it contains more data points in the open phase than the adsorption branch. Once K and N have been determined by direct fitting, our goal is to calculate the value of the free energy difference, ΔF, from the transition pressure. We can do this because, at the thermodynamic equilibrium between the two phases, we have:

$$\Delta\Omega = 0$$

This allows us to link the transition pressure, at thermodynamic equilibrium, to the other parameters (N, K, ΔF) in the following manner:

$$P_{\text{trans}} = \frac{N}{K}\left(e^{-\frac{\Delta F}{NRT}} - 1\right)$$

Because there is a hysteresis in the adsorption–desorption isotherms, we cannot directly extract the value of thermodynamic equilibrium P_{trans} from the isotherms. We know it is bracketed by the gate closing (P_{gc}) and gate opening (P_{go}) pressures, respectively — and the trends observed are valid, whether we should choose to approximate P_{trans} by either value. In the present work, we have chosen based on thermodynamic arguments to use $P_{\text{trans}} = (P_{\text{go}} \times P_{\text{gc}})^{1/2}$.

Supplementary **Table 3**. **Parameters calculated for the thermodynamic model of adsorption of acetylene (C_2H_2) at 273 K in MOF-508 and its derivatives.**

	N (mol/mol)	K (kPa^{-1})	P_{go} (kPa)	P_{gc} (kPa)	P_{trans} (kPa)	ΔF (kJ/mol)
MOF-508	2.872	0.550	45.4	16.7	27.5	5.2
$(NH_2)_{10}$-MOF-508	2.769	0.497	51.7	18.2	30.7	5.1
$(NH_2)_{20}$-MOF-508	2.747	0.430	60.9	21.2	35.9	5.1
$(NH_2)_{40}$-MOF-508	2.268	0.318	83.2	22.6	43.4	4.4
$(NO_2)_{20}$-MOF-508	2.636	0.421	12.1	10.2	11.1	2.6
$(NO_2)_{50}$-MOF-508	2.661	0.389	6.5	7.0	6,7	1.8
$(NO_2)_{100}$-MOF-508	2.484	0.286	1.0	0.9	0.96	0.3

Supplementary **Figure 37.** Acetylene adsorption at 195 K of a) ***100%*-NO$_2$-MOF** b) **MOF-508** and c) ***100%*-NH$_2$-MOF** and related in-situ PXRD of d) ***100%*-NO$_2$-MOF** e) **MOF-508** and f) ***100%*-NH$_2$-MOF**.

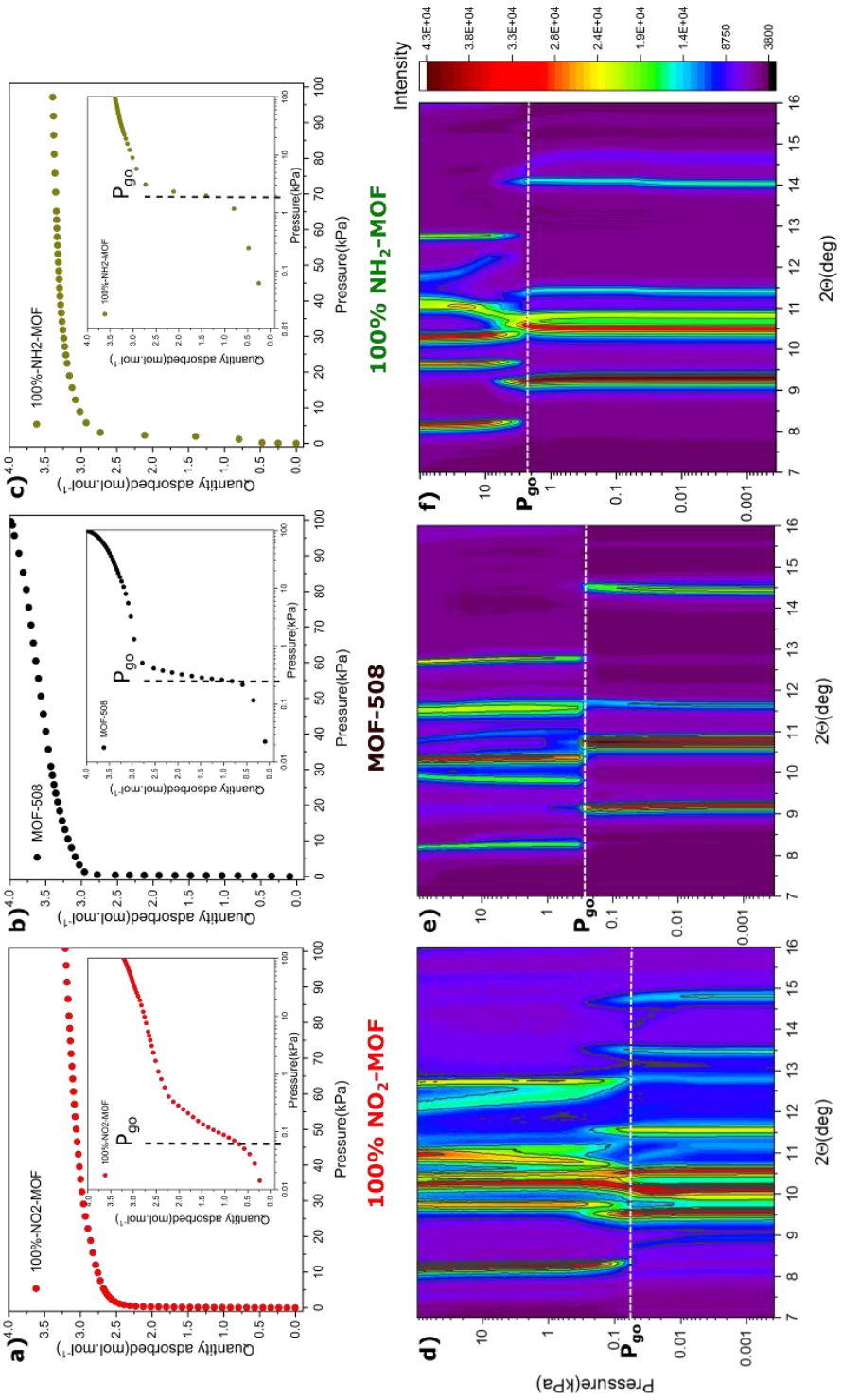

Supplmentary **Table 4.** Comparison of acetylene total volumetric useable capacity (v/v) for **MOF-508** and **$(NH_2)_{60}$-MOF-508**, and a selection of the best reported MOFs. The maximum adsorption pressure is 100kPa and the minimum desorption pressure is 70 kPa.

Framework	Total amount 273 K-120 k v/v	Total amount 298–70 kPa v/v	Useable amount 298 K-70 kPa v/v	% Amount released	Reference
MOF-508	129	70	60	46	This work
$(NH_2)_{60}$-MOF-508	126	20	106	84	This work
Dps-VCo-BDC (CPM-733-dps)	204	161	127	62	10.1002/anie202008696
ZJU-12a	240	124	116	48	10.1039/c6ce02291j
NOTT-101	198	99	99	50	10.1039/C2EE22858K
PCN-16	194	108	86	44	10.1039/C2EE22858K
UTSA-20	195	118	77	39	10.1039/C2EE22858K
CuBTC-HKUST-1	228	154	74	32	10.1039/C2EE22858K
MOF-505	176	111	65	37	10.1039/C2EE22858K
NOTT-102	132	67	65	49	10.1039/C2EE22858K
UMCM-150	127	67	60	47	10.1039/C2EE22858K
FJI-H8	240	183	57	24	10.1038/ncomms8575
ZJU-5	179	128	51	28	10.1039/C5RA12700A
MgMOF-74	204	159	45	22	10.1039/C2EE22858K
CoMOF-74	240	199	41	17	10.1039/C2EE22858K

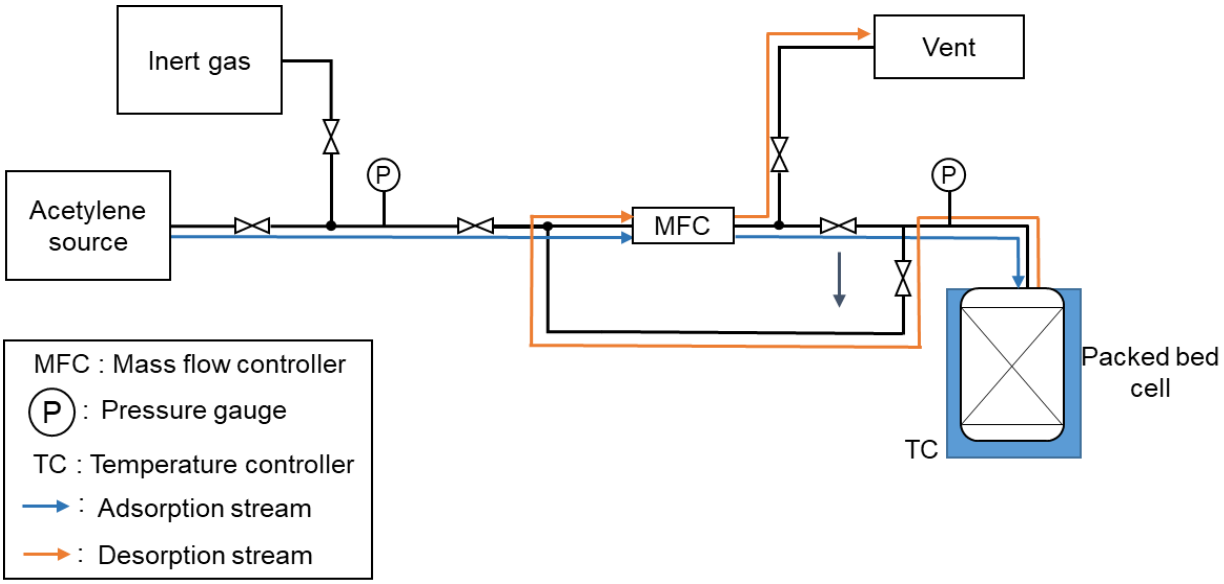

Supplementary **Figure 38.** Representation of the acetylene storage experimental setup

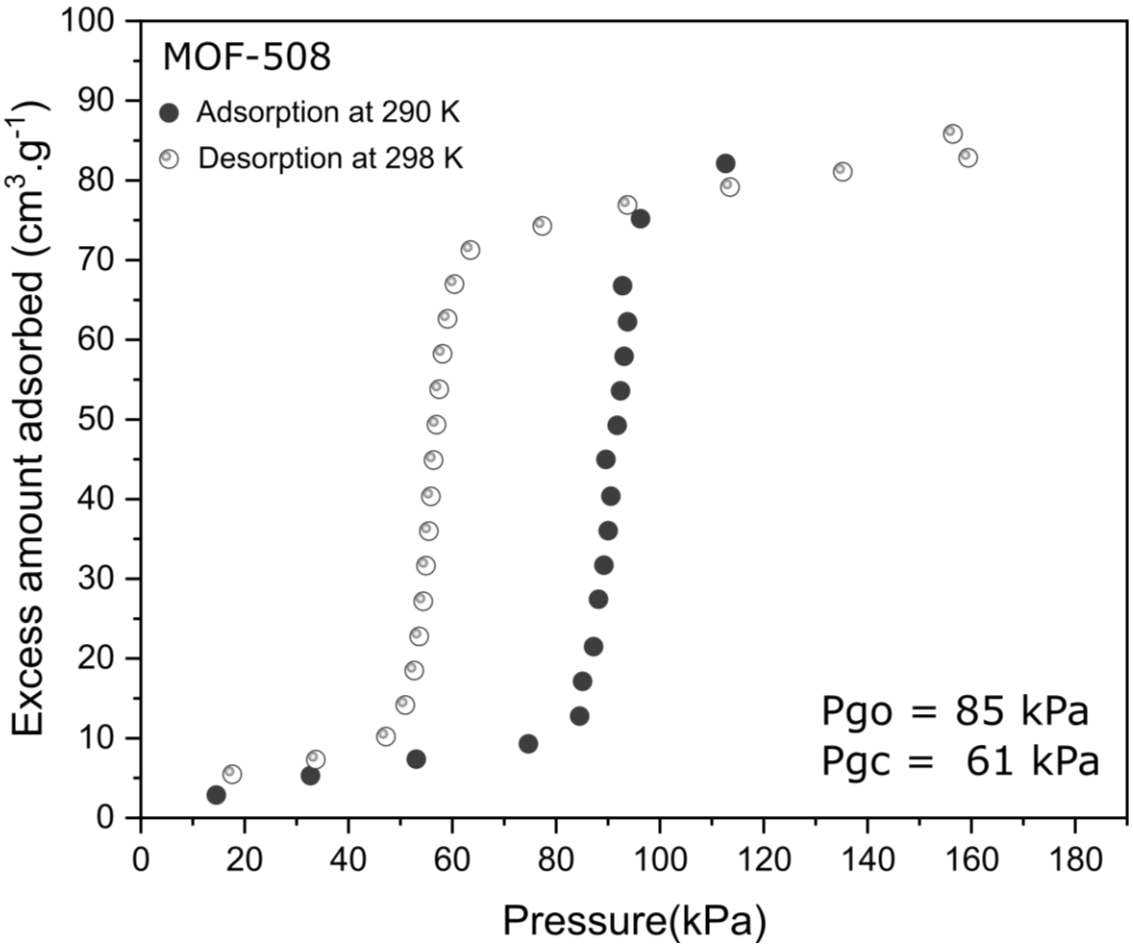

Supplementary **Figure 39.** Acetylene (C_2H_2) adsorption isotherm (filled symbols) at 290 K followed by a desorption isotherm (empty symbols) at 298 K for **MOF-508**

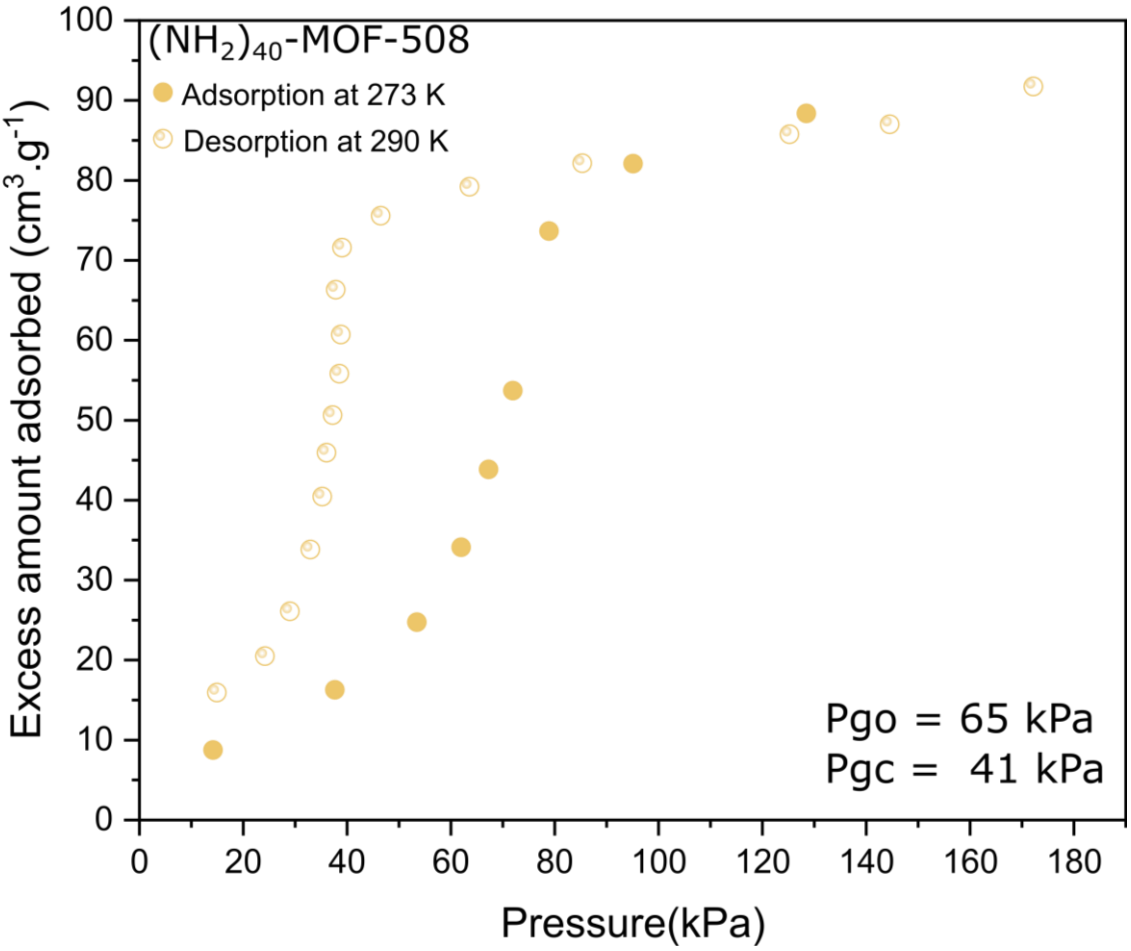

Supplementary **Figure 40.** Acetylene (C_2H_2) adsorption isotherm (filled symbols) at 273 K followed by a desorption isotherm (empty symbols) at 290 K for **$(NH_2)_{40}$-MOF-508**

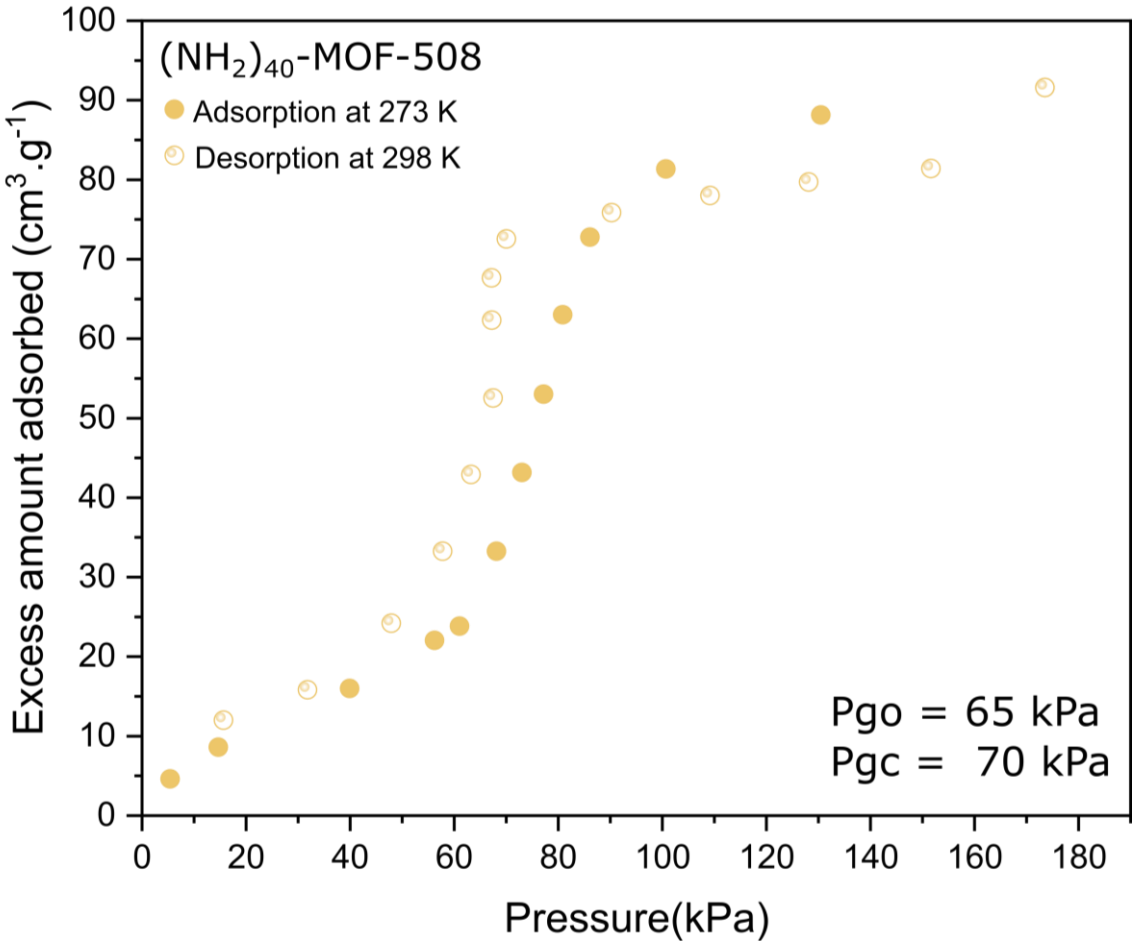

Supplementary **Figure 41.** Acetylene (C_2H_2) adsorption isotherm (filled symbols) at 273 K followed by a desorption isotherm (empty symbols) at 298 K for **$(NH_2)_{40}$-MOF-508**

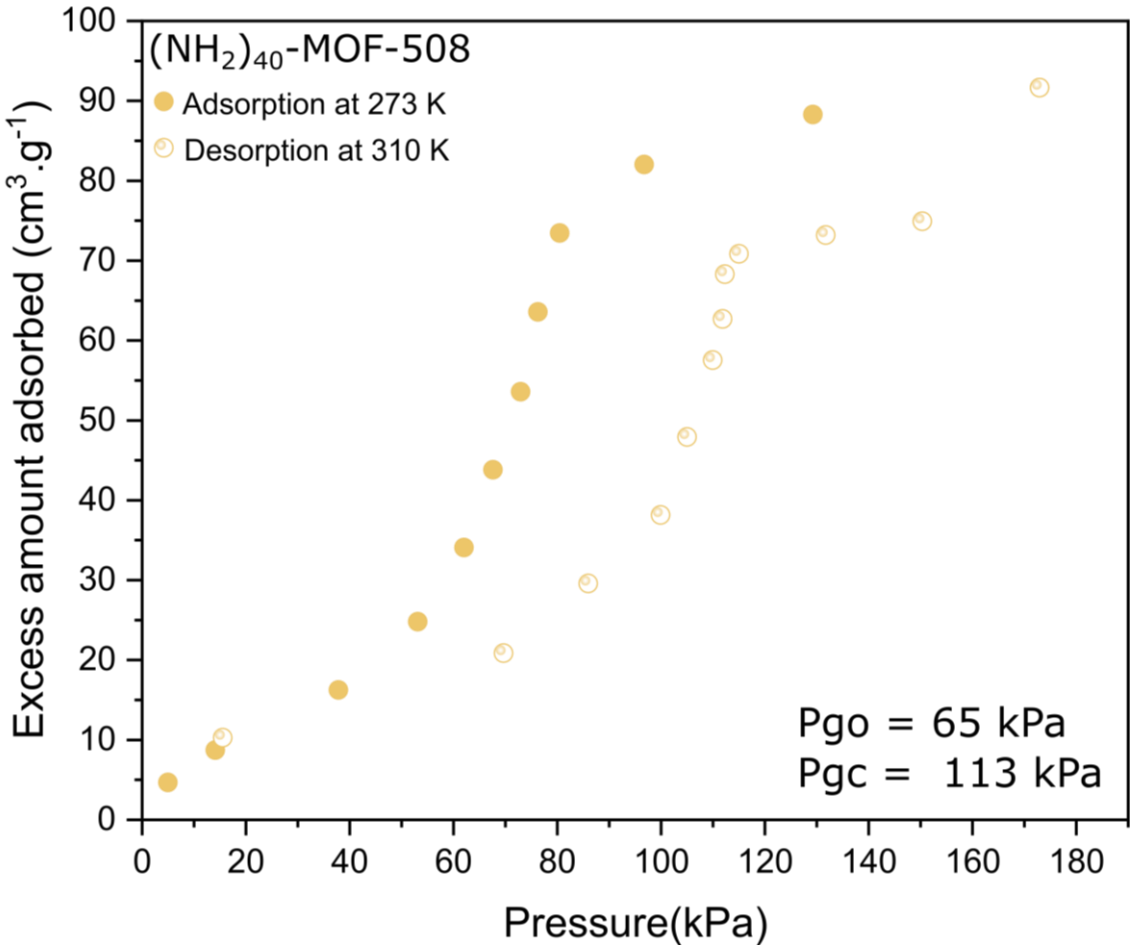

Supplementary **Figure 42.** Acetylene (C_2H_2) adsorption isotherm (filled symbols) at 273 K followed by a desorption isotherm (empty symbols) at 310 K for **$(NH_2)_{40}$-MOF-508**

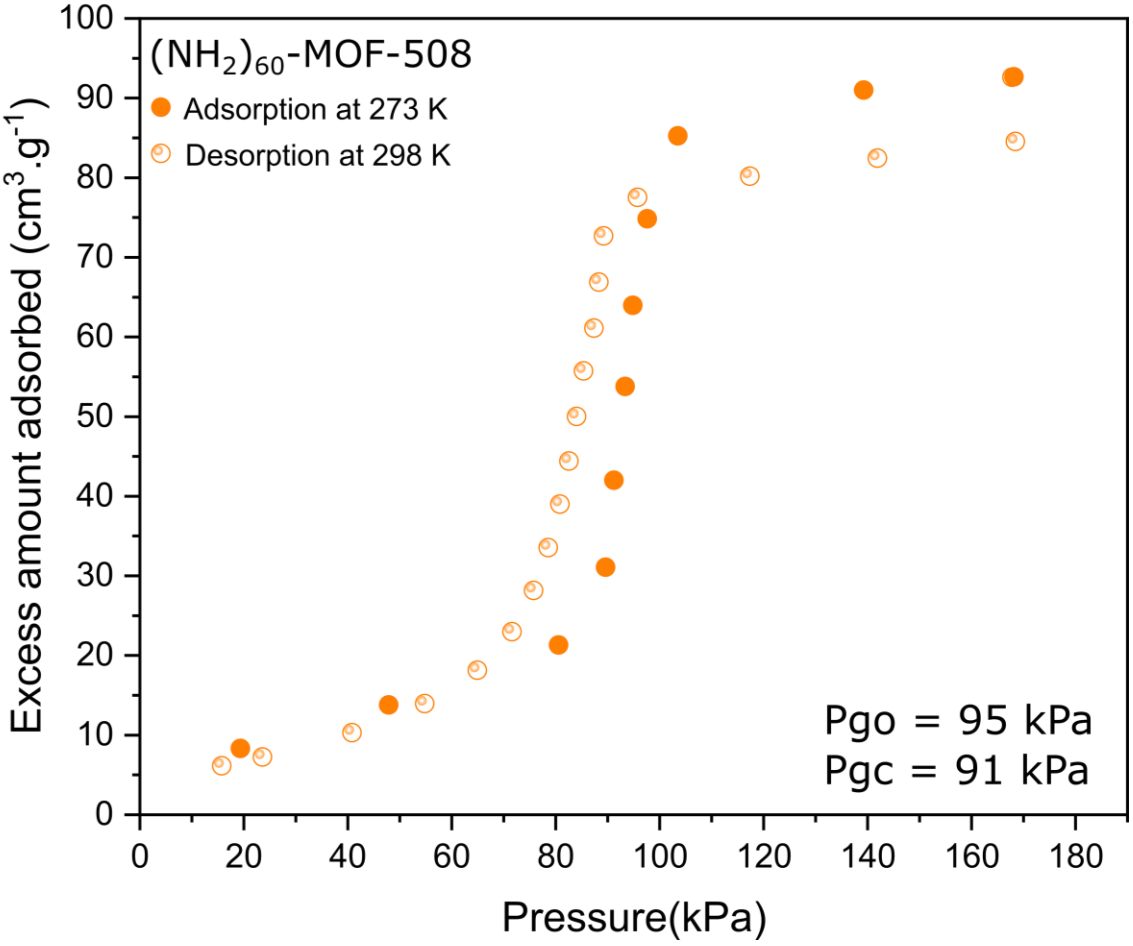

Supplementary **Figure 43.** Acetylene (C_2H_2) adsorption isotherm (filled symbols) at 273 K followed by a desorption isotherm (empty symbols) at 298 K for **$(NH_2)_{60}$-MOF-508**

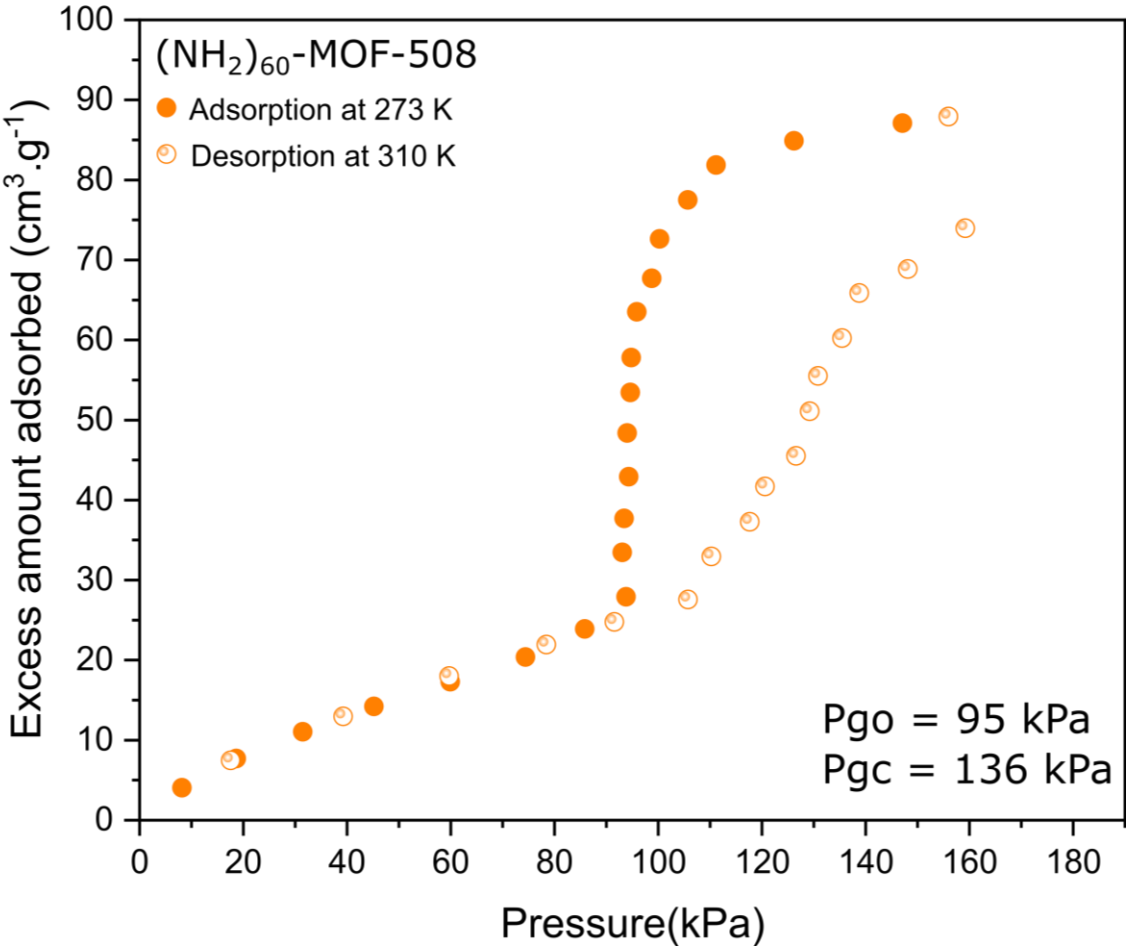

Supplementary **Figure 44.** Acetylene (C_2H_2) adsorption isotherm (filled symbols) at 273 K followed by a desorption isotherm (empty symbols) at 310 K for **$(NH_2)_{60}$-MOF-508**

Refrences

1. Bousquet, D.; Coudert, F.-X.; Fossati, A. G. J.; Neimark, A. V.; Fuchs, A. H.; Boutin, A., Adsorption induced transitions in soft porous crystals: An osmotic potential approach to multistability and intermediate structures. *J. Chem. Phys., 138* (17), 174706 (2013).
2. Coudert, F.-X.; Jeffroy, M.; Fuchs, A. H.; Boutin, A.; Mellot-Draznieks, C., Thermodynamics of Guest-Induced Structural Transitions in Hybrid Organic−Inorganic Frameworks. *Journal of the American Chemical Society* **2008,** *130* (43), 14294-14302.
3. Coudert, F.-X.; Mellot-Draznieks, C.; Fuchs, A. H.; Boutin, A., Double Structural Transition in Hybrid Material MIL-53 upon Hydrocarbon Adsorption: The Thermodynamics Behind the Scenes. *Journal of the American Chemical Society* **2009,** *131* (10), 3442-3443.
4. Coudert, F.-X., The osmotic framework adsorbed solution theory: predicting mixture coadsorption in flexible nanoporous materials. *Physical Chemistry Chemical Physics* **2010,** *12* (36), 10904-10913.